AD-A194 805 MODEL STUDIES OF CBES (CHEMICALLY BOUND EXCITED STATES) 1/1
DECOMPOSITION..(U) ROCKWELL INTERNATIONAL THOUSAND OAKS
CA SCIENCE CENTER D J BENARD ET AL. FEB 88 SC5467.0SR
UNCLASSIFIED AFAL-TR-87-071 F04611-86-C-0072 F/G 7/2 NL

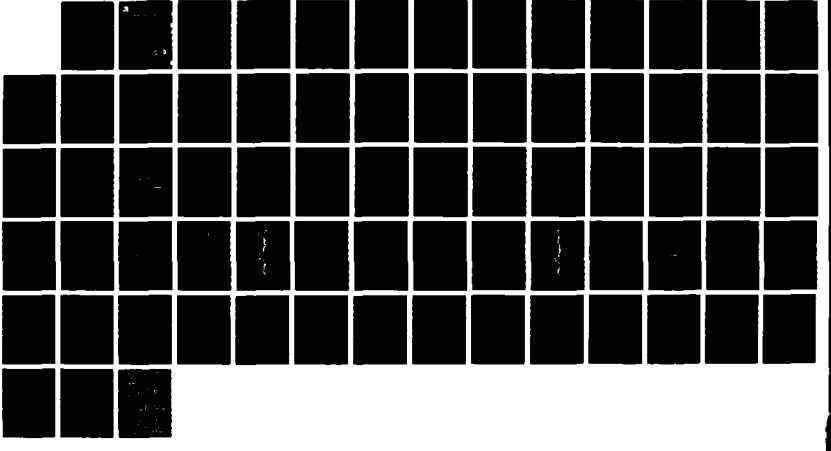

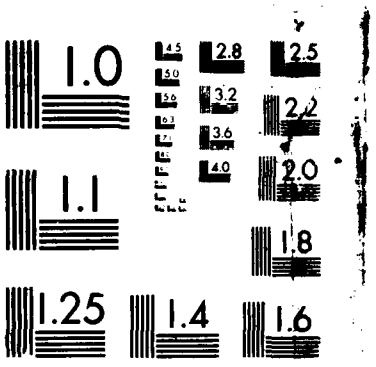

(4)

AFAL-TR-87-071

AD:

Interim Report
for the period
1 May 1987 to
31 July 1987

Model Studies of CBES Decomposition

AD-A194 805

February 1988

Authors:
D. J. Benard
R. H. Cohn

Rockwell International
Science Center
1049 Camino Dos Rios
Thousand Oaks, CA 91360

F04611-86-C-0072

Approved for Public Release

Air Force Astronautics Laboratory

Air Force Space Technology Center
Space Division, Air Force Systems Command
Edwards Air Force Base,
California 93523-5000

NOTICE

When U.S. Government drawings, specifications, or other data are used for any purpose other than a definitely related government procurement operation, the government thereby incurs no responsibility nor any obligation whatsoever, and the fact that the government may have formulated, furnished, or in any way supplied the said drawings, specifications, or other data, is not to be regarded by implication or otherwise, or conveying any rights or permission to manufacture, use, or sell any patented invention that may in any way be related thereto.

FOREWORD

This interim report was submitted by Rockwell International's Science Center in Thousand Oaks, CA, in support of contract F04611-86-C-0072 with the Air Force Astronautics Laboratory (AFAL), Edwards Air Force Base, CA. AFAL Project Manager was 1Lt Walt Lauderdale.

This report has been reviewed and is approved for distribution in accordance with the the distribution statement on the cover and on the DD Form 1473.

Walter J. Lauderdale

WALTER J. LAUDERDALE, 1Lt, USAF
Project Manager

FOR THE COMMANDER

Robert C. Corley

ROBERT C. CORLEY
Chief, ARIES Office

SECURITY CLASSIFICATION OF THIS PAGE

REPORT DOCUMENTATION PAGE

Form Approved OMB No. 0704-0188

1a. REPORT SECURITY CLASSIFICATION: UNCLASSIFIED	1b. RESTRICTIVE MARKINGS
2a. SECURITY CLASSIFICATION AUTHORITY	3. DISTRIBUTION/AVAILABILITY OF REPORT: Approved for public release; distribution is unlimited.
2b. DECLASSIFICATION/DOWNGRADING SCHEDULE	
4. PERFORMING ORGANIZATION REPORT NUMBER(S): SC5467.QSR	5. MONITORING ORGANIZATION REPORT NUMBER(S): AFAL-TR-87-071
6a. NAME OF PERFORMING ORGANIZATION: Rockwell International Science Center; 6b. OFFICE SYMBOL (If applicable):	7a. NAME OF MONITORING ORGANIZATION: Air Force Astronautics Laboratory
6c. ADDRESS (City, State, and ZIP Code): 1049 Camino Dos Rios, Thousand Oaks, CA 91360	7b. ADDRESS (City, State, and ZIP Code): AFAL/CX, Edwards Air Force Base, CA 93523-5000
8a. NAME OF FUNDING/SPONSORING ORGANIZATION; 8b. OFFICE SYMBOL (If applicable):	9. PROCUREMENT INSTRUMENT IDENTIFICATION NUMBER: F04611-86-C-0072
8c. ADDRESS (City, State, and ZIP Code):	10. SOURCE OF FUNDING NUMBERS

PROGRAM ELEMENT NO.	PROJECT NO.	TASK NO	WORK UNIT ACCESSION NO.
62302F	5730	00	WM

11. TITLE (Include Security Classification): Model Studies of CBES Decomposition (U)

12. PERSONAL AUTHOR(S): Benard, D. J., and Cohn, R. H.

13a. TYPE OF REPORT	13b. TIME COVERED	14. DATE OF REPORT (Year, Month, Day)	15. PAGE COUNT
Interim	FROM 87/5/1 TO 87/7/31	88/2	70

16. SUPPLEMENTARY NOTATION

17. COSATI CODES		
FIELD	GROUP	SUB-GROUP
07	04	
21	09	

18. SUBJECT TERMS (Continue on reverse if necessary and identify by block number): Fluorine azide, nitrogen fluoride, chemically bound excited states, diatomic molecules, detonation, decomposition and dissociation reactions, electronic and vibrational excitation, metastable states, energy storage, transfer and pooling, emission spectra, kinetics, potential energy curves, high impulse propellants

19. ABSTRACT (Continue on reverse if necessary and identify by block number)

The molecule FN_3, known as fluorine azide is a stabilized complex of excited singlet NF and N_2, similar to other theoretically predicted molecules which are of interest as high impulse rocket propellants. Since little is known about the decomposition of these materials in condensed phases we have begun a study of the laser initiated detonation of thin films of FN_3. It is hoped that analysis of the resulting emissions will yield a better understanding of the mechanisms which control release of the stored electronic/chemical energy. This report covers the first of three years work which includes development of an FN_3 source and an apparatus to form and detonate FN_3 films and collect emission spectra with μs temporal resolution. Data collected to date has shown that detonation of FN_3 results in chemiluminescence at visible and near ultraviolet wavelengths. The emissions appear to be diatomic in origin and are most intense in the 350-500 nm wavelength range, but do not correspond to any of the known band systems of N_2 or NF. These new spectroscopic features may result from energy pooling reactions between metastable NF intermediates, produced by the explosive decomposition of the FN_3 molecules.

20. DISTRIBUTION/AVAILABILITY OF ABSTRACT	21. ABSTRACT SECURITY CLASSIFICATION
☒ UNCLASSIFIED/UNLIMITED ☐ SAME AS RPT. ☐ OTIC USERS	UNCLASSIFIED

22a. NAME OF RESPONSIBLE INDIVIDUAL	22b. TELEPHONE (Include Area Code)	22c. OFFICE SYMBOL
Walter J. Lauderdale, 1LT, USAF	(805) 275-5413	CX

DD Form 1473, JUN 86 — Previous editions are obsolete. — SECURITY CLASSIFICATION OF THIS PAGE

TABLE OF CONTENTS

LIST OF FIGURES

LIST OF FIGURES (continued)

INTRODUCTION AND SUMMARY

The molecule FN_3, known as fluorine azide, was discovered in 1942 by Haller, who synthesized it by reacting HN_3 with F_2. Haller found that FN_3 was a volatile gas that was easily detonated when condensed at cryogenic temperature. Haller also observed that FN_3 always reacted by central bond rupture.[1] Our involvement with FN_3 began in 1983 with a study of its photolysis by an ArF laser, which demonstrated a singlet ground state and a heat of formation of 120-135 kcal/mole.[2] More recently, Gholivand et al have precisely measured the physical properties of FN_3, including the infrared and visible/ultraviolet absorption spectra, the vapor presure curve and the freezing point.[3] Michels has also recently performed an ab initio calculation of the FN_3 ground state potential energy surface which yielded thermodynamic values and vibrational frequencies in good agreement with the experimental data. Michels' calculation shows that there is a large barrier to dissociation of the $F\text{-}N_3$ bond, while the $FN\text{-}N_2$ bond is much weaker.[4] Most recently, as part of our IR&D program,[5] we showed experimentally that transfer of vibrational energy from HF or DF to FN_3 rapidly dissociates the molecule and liberates metastable $NF(a^1\Delta)$ with high efficiency.

These observations can be explained in terms of the potential surfaces that are illustrated in Fig. 1, where the states of FN_3 are composed from the separated states of NF and N_2 by treating the central bond as a perturbation which varies in strength as a function of internuclear separation. The triplet state correlating to $N_2(X^1\Sigma) + NF(X^3\Sigma)$ is highly repulsive because it mixes with a triplet surface that correlates to the excited metastable $N_2^*(A^3\Sigma)$ state. Physically, as NF(X) and N_2(X) are brought into contact, some of the triplet character originally associated with the NF(X) is redistributed to the N_2 molecule. Since the lowest triplet state in N_2 is highly excited, this interaction is strongly repulsive. The interaction of the metastable $NF^*(a^1\Delta, b^1\Sigma)$ states with N_2(X) would normally yield a Van der Waals-type interaction on a singlet surface. The interaction of NF(X) with N_2^*(A), however, also yields a singlet surface which is strongly attractive due to spin cancellation. The two singlet surfaces interact via an "avoided crossing" which generates a stable well in the lower potential energy surface. The lowest triplet state must pass above this potential well, since otherwise FN_3 would decay radiatively to the repulsive triplet state and then dissociate spontaneously. Therefore,

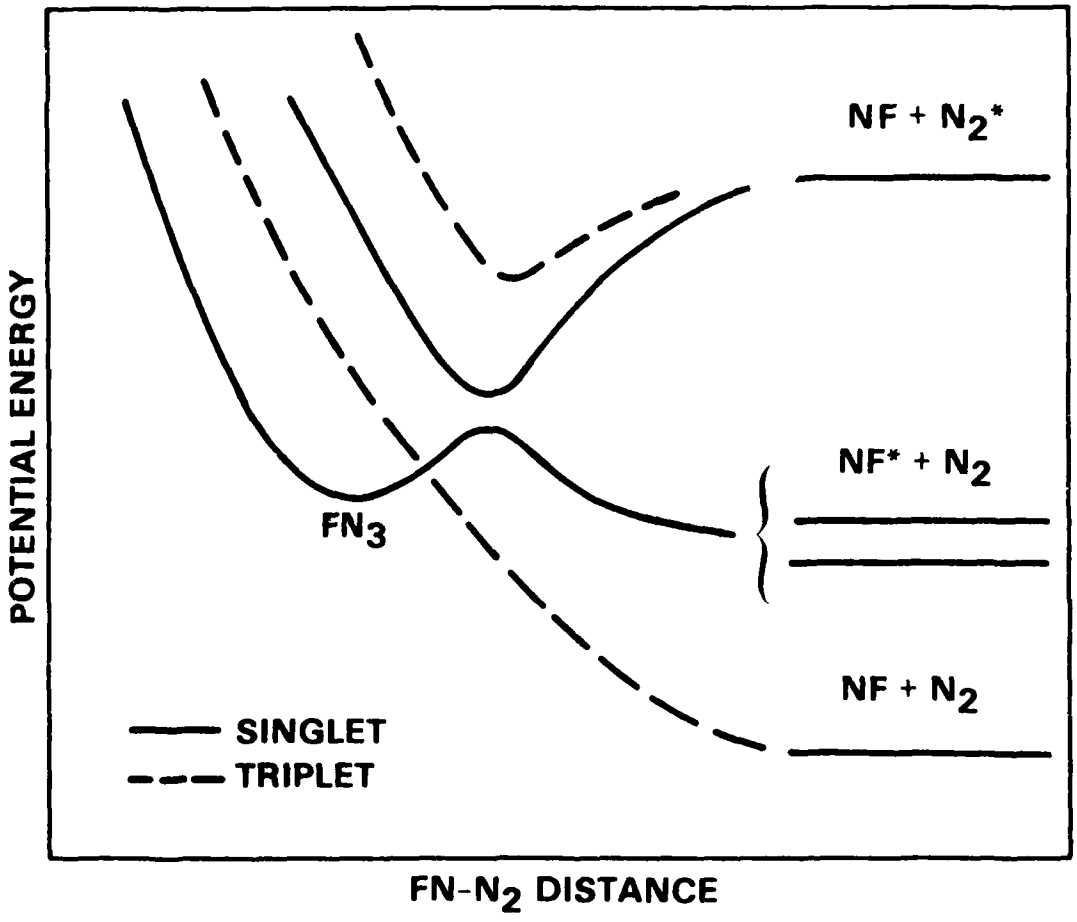

Fig. 1 Approximate illustration of FN_3 potential energy surfaces.

the ground state of FN_3 must be a singlet which dissociates to metastable NF*(a,b) and ground state N_2. In physical terms, FN_3 traps the electronic excitation energy of NF*(a,b) because a photon transition to the lower triplet surface that dissociates to NF(X) requires a significant change of the nuclear coordinates. Since photons carry virtually no momentum, radiative decay is strictly forbidden.

Molecules, such as FN_3, which are stabilized complexes of smaller molecules not in their ground states, are known as chemically bound excited states (CBES). These molecules find application as high impulse rocket propellants because of their inherent energy storage capabilities. Most of the work on CBES technology has to date been theoretical and has focused on the potential energy surfaces of isolated molecules. Consequently, there is little knowledge concerning the problem of detonation that is inherent to CBES systems in condensed phases. Since the ground states of CBES molecules are correlated to elecronically excited fragments, detonation waves can be propagated by electronic energy transfer and photon emission-absorption reactions in addition to the usual thermal mechanisms. Therefore, experimental efforts on existing CBES materials are required to address this critical issue.

This work studies the production and role of electronically excited species in condensed FN_3 detonations with the goal of gaining insight on effective stabilization techniques. The basic experiment involves generating FN_3 gas, forming a thin film on a transparent substrate at low temperature, detonating the film via a pulsed laser and applying spectroscopic and kinetic diagnostic tools to monitor the excited state concentrations. The work is planned in three phases each of twelve months duration. In the first phase, the goals are to assemble and debug apparatus for the reproducible production and detonation of FN_3 films and to apply emission spectroscopy to characterize the radiation resulting from the generation of electronically excited species. The second phase builds upon the first by gathering temporally resolved emission and absorption data to uncover the mechanism of the detonation and identify potential stabilization methods. In Phase 3, the time resolved diagnostics developed in Phase 2 will be applied to assess the effectiveness of the various stabilization techniques. It is anticipated that the time profiles of key excited state species will be influenced by the presence of effective stabilizers before actual stability against detonation is achieved.

This report marks the successful conclusion of Phase I. The significant results include:

1. Demonstration of a generator which delivers approximately 2 - 3% FN_3 in He at 350 torr total pressure and 3.5 sccs flow rates for up to 3 hours with less than ± 10% variation in the FN_3 yield and impurities less than 1% of the FN_3 concentration. The FN_3 source is equipped with on-line diagnostics to monitor its performance at each stage of the synthesis so that corrections can be applied in real time.

2. Development of a coldfinger apparatus for the reproducible production and laser detonation of FN_3 films of approximately 5 - 10 μm thickness on transparent substrates. The films were most easily formed and detonated on plasma-cleaned CaF_2 substrates at liquid nitrogen temperature.

3. The emission spectra from detonation of the FN_3 films were significantly influenced by the accuracy of the titration of F_2 with HN_3 used to generate the FN_3 and by plasma cleaning of the substates prior to deposition of the films, while dependence on substrate material (CaF_2 or SiO_2) and the use of a cold trap to purify the FN_3 flow was not easily detected. From these observations, it was concluded that the substrates were not chemically active in the detonations and that the emissions produced by detonation of cold-trap purified FN_3 films did not result from impurities in the FN_3 gas stream.

4. The emission spectrum from detonation of cold-trap purified FN_3 films was most intense at near-ultraviolet wavelengths. Less intense emissions were observed in the visible spectrum and no emission was detected out to 900 nm in the near-infrared. The ultraviolet emissions were diatomic in origin and did not correspond to any of the known band systems of N_2 or F_2. A weak band from 500-525 nm was assigned to radiation from

high vibrational levels of the NF(b) state to the corresponding levels of the NF(X) ground state.[6]

5. Consideration of the NF potential energy curves[7] shows that the ultraviolet emissions could result from energy pooling reactions which populate higher excited states of NF or from the transient formation and radiative decay of the NF(a) • NF(a) dimol. Other observations, regarding the operation of the coldfinger and observance of similar spectra in a flow tube reactor suggests that some of these emissions may be due to impurities that were generated within the coldfinger apparatus itself. Steps to resolve these uncertainties, including mass spectrum analysis of the FN_3/He gas stream, modification of the coldfinger apparatus and collection of reference spectra for comparison purposes were planned for early in Phase 2.

The following section contains a detailed description of the experimental apparatus and procedures. Following this, the spectroscopic data are reviewed and interpreted and plans for the kinetic investigation of Phase 2 are presented. Finally, preliminary data, gathered under Phase 2, has been included since it has a bearing on the interpretation of the Phase 1 results.

EXPERIMENTAL DETAILS

The following subsections contain information relative to the safe generation of FN_3 gas, the reproducible formation and detonation of FN_3 films and the detection system employed to gather the resulting emission spectra. In developing the apparatus, some specialized electronic circuits were required to accomplish certain control and timing functions. The operation of these circuits can be appreciated only with a suitable background in electrical engineering. Therefore, the principles relating to their design will not be discussed. Schematics of the circuits are given, however, in sufficient detail to allow easy replication. The designs are noncritical with respect to layout, tolerance of components and supply voltage.

Safety Considerations

Before proceeding, we feel it important to warn potential experimenters that FN_3 is a chemical which deserves much respect. Its energy storage per unit mass is twice that of TNT and it is highly sensitive in its liquid state. Haller reports that the explosions of FN_3 were very brissant, that it was harder to keep liquid FN_3 from detonating than not, and that detonation of as little as one drop of FN_3 pulverized glassware up to 25 cm away and at closer distances drove small pieces of glass through 24 gauge steel. Haller also noted that slight mechanical vibration or simple evaporation of the liquid were sufficient to cause detonation of FN_3.[1] From our own experiments, we can say that Haller did not exaggerate. In our laboratory, detonations of microscopically thin films of FN_3 have cracked 0.25 in. thick substrates of both CaF_2 and SiO_2.

To handle FN_3 safely, particular care must be exercised to prevent condensation of any significant quantity of the liquid or reaction of the FN_3 gas with other materials. Haller reports that FN_3 gas is adsorbed irreversibly on KF at room temperature to form a compound that explodes upon heating[1] and we have found that passage of FN_3 gas over copper generates an explosive film, most likely copper azide. By keeping the FN_3 concentrations below 10 torr, using only glass, teflon or stainless steel for construction, and avoiding condensation except of microscopically thin films, we were able to prevent accidental explosions, although flashbacks were occassionally

observed in teflon lines carrying the FN_3 gas. Nonetheless, we recommend the use of blast shields, sand fills, barracades and other safety features, as discussed in the following subsection.

The HN_3 that is produced as an intermediate to the generation of FN_3 has similar explosive tendencies and requires equal attention to safety.[8] Procedures for handling NaN_3, used as a starting material, are available from the manufacturer.[9] While less energetic that FN_3 or HN_3, NaN_3 is still an exothermic material that is capable of spontaneous decomposition if activated by excess heat or friction. Also, NaN_3 can react with acids to form HN_3 and with metals to form explosive metal azides. All azides are highly toxic, thus care must be taken to prevent exposure. Finally, the use of even dilute F_2 can be hazardous if handled improperly. Instructions for the safe use of F_2 are typically available from the manufacturer.[10]

Synthesis of Fluorine Azide

Fluorine azide was synthesized in a continuous manner using the method of Haller,[1] by reacting HN_3 with F_2, with some variations, as shown in Fig. 2. The HN_3 was generated by the thermally activated reaction of NaN_3 with stearic acid[11] rather than dilute H_2SO_4. This approach had the advantage of producing a bone-dry flow of HN_3 in contrast to the sulfuric acid reaction which requires a downstream trap to remove water vapor. From previous experiments using the sulfuric acid technique, we found that explosive compounds built up around metal fittings between the HN_3 generator and a trap that was filled with $CaSO_4$. We also noticed that the $CaSO_4$ significantly attenuated the HN_3 flow which raised the possibility of explosive compound formation in the trap. Finally, we found that the NaN_3-stearic acid reaction was smoother, more predictable and easier to clean up safely than the sulfuric acid technique.

<u>HN_3 Generator</u> - Figure 3 is a cross sectional view of the HN_3 generator assembly. A 2-liter Kimax reaction kettle containing the NaN_3 and stearic acid was supported inside a 400 W electric deep fat fryer by a stainless steel support structure. The pot was filled with cooking oil whose temperature (T_1) was measured by a metal band thermometer. Stainless steel cooling coils in the annulus between the reaction kettle and the pot were

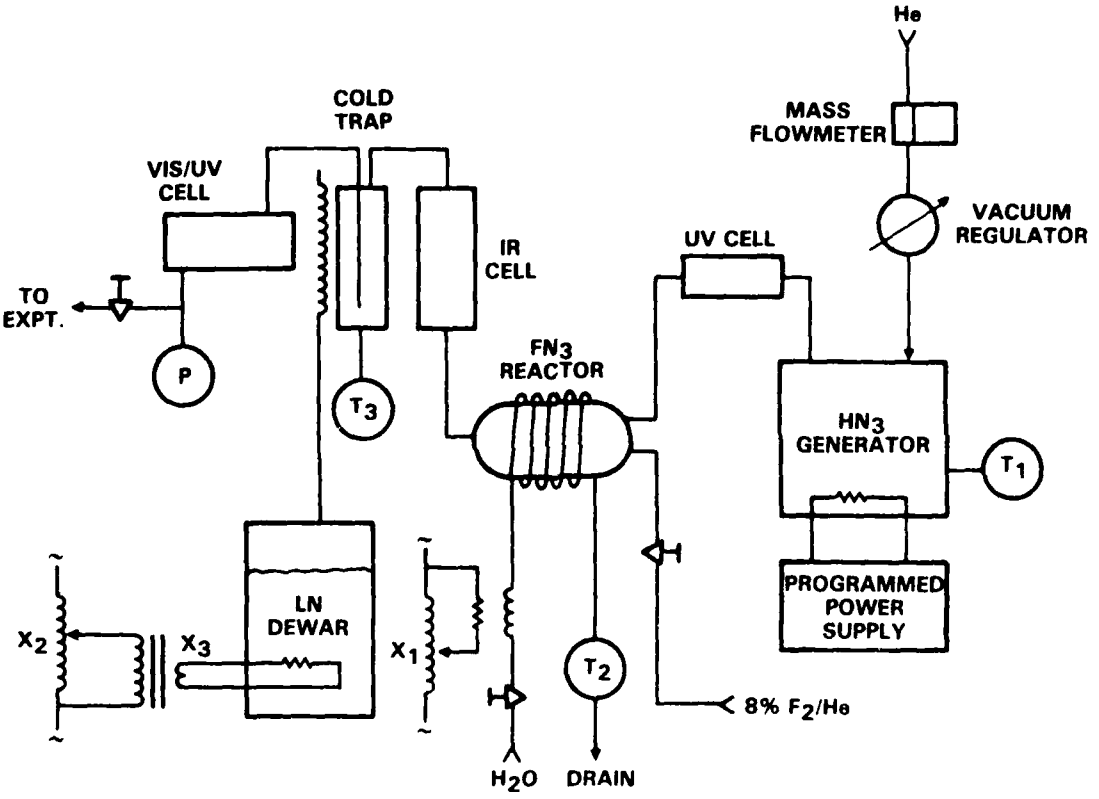

Fig. 2 Schematic of apparatus for synthesis of FN_3 gas.

also attached to a source of tap water. Water was admitted to this structure only for the purpose of cooling the oil to stop the NaN_3-stearic acid reaction in an emergency or at the end of a day's run. A heavy stainless steel lid, atop the reaction kettle, was sealed to the ground glass mating surface of the kettle by an O-ring. The He carrier gas entered the reaction kettle via an electronic mass flowmeter, a vacuum regulator and the steel lid, mixed with the evolving HN_3 inside the kettle and exited via a second line through the lid. The regulator was set to maintain 350 torr absolute pressure inside the kettle and the He flow was approximately 3.5 sccs. Also, atop the lid, a 1 RPM gear motor with 600 in. oz. torque rating was mated to a teflon lined paddle inside the kettle via an O-ring seal on the shaft. Operation of the HN_3 generator without stirring caused the HN_3 yield to fall off quickly, which raised concerns about potential buildup of high HN_3 concentrations in the stearic acid melt and the possibility of explosion. The entire HN_3 generator assembly was operated inside an 0.25 in. thick lexan blast shield located inside a conventional fume hood.

<u>FN_3 Generator</u> - Contrary to Haller's thesis,[1] we found copper to be incompatible with FN_3 in that mixing of HN_3 and F_2 over copper shot produced very little FN_3, but the shot became coated with a greenish layer which exploded when struck forcefully with a hammer. Therefore, the FN_3 was formed inside an 0.6 liter stainless steel cylinder packed with 0.25 in. dia. stainless steel balls. The HN_3/He flow was admitted to this reactor along with an adjustable flow of 8 - 10% F_2 in He through a nozzle which prevented rapid mixing of the reagents. A copper tube carrying resistively-heated tap water was soldered onto the exterior of the steel cylinder to maintain the reactor at constant temperature. The water was heated by passage over a brass block in which two 1000 W cartridge heaters were inserted and connected in parallel to a Variac (X_1) The temperature of the water (T_2) was measured by a metal band thermometer as it exited from the reactor to a drain. Consistent with Haller's work, we found that the highest FN_3 yields were obtained at 35°C with substantial reduction below 20°C or above 50°C.

<u>Cold Trap</u> - Downstream of the secondary reactor, the gas stream was passed through a cold trap to remove the HF by-product of the FN_3 and any residual HN_3. Early experiments which utilized a NaF trap were discontinued because the FN_3 was severely attenuated which raised the possibility of eventual detonation. The cold trap was

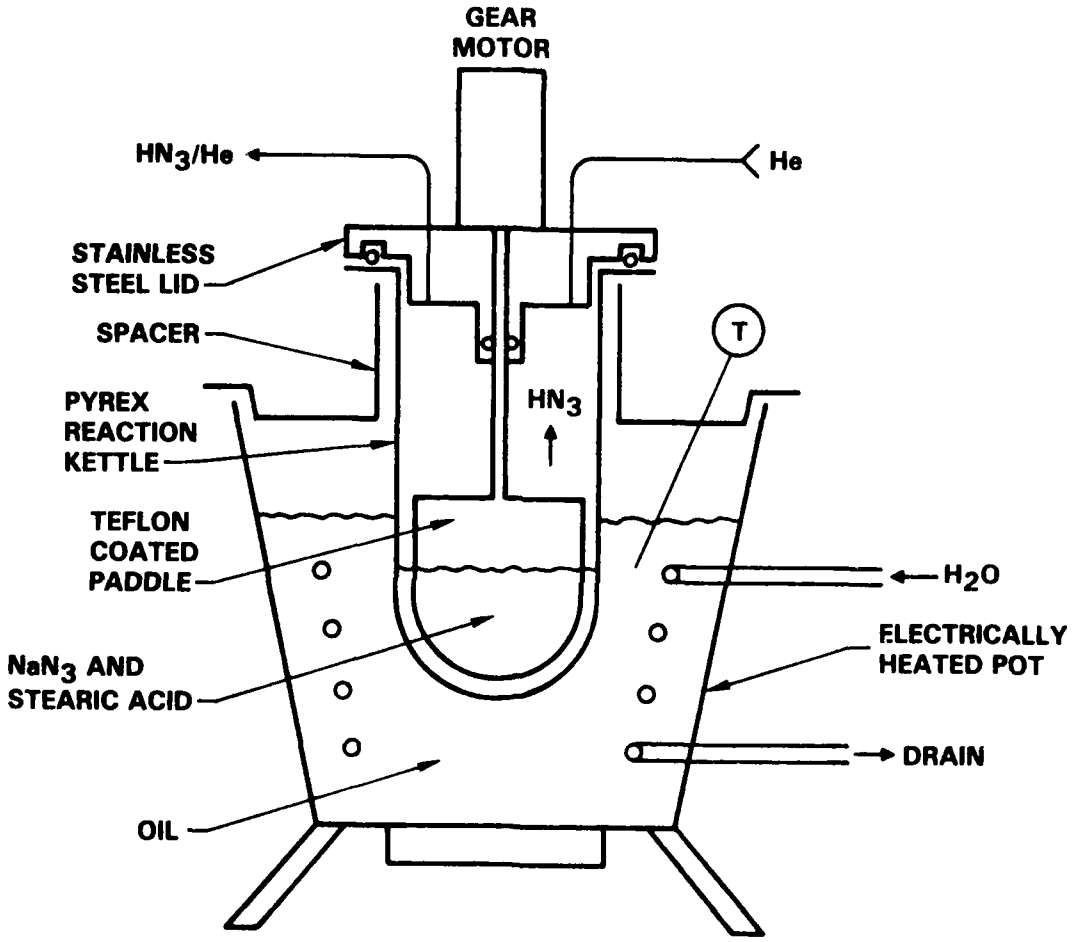

Fig. 3 Detailed view of HN_3 generator.

constructed of a 0.3 liter stainless steel cylinder with a dip tube and 1/4 in. stainless steel balls in the bottom third. A copper cooling coil soldered to the exterior of the trap was connected via insulted lines to a sealed 5 liter liquid nitrogen dewar. Two 50 W, 10 Ω power resistors in the bottom of the dewar were used to boil off gaseous nitrogen at 77 K to cool the trap remotely. The lid of the dewar was spring loaded so that it would lift off and relieve pressures in excess of 6 psig. The temperature at the base of the trap (T_3) was monitored via a thermocouple gauge and meter. The resistive heater for the liquid nitrgen dewar was powered by a Variac (X_2) and a 120 to 24 V stepdown transformer (X_3) rated at 100 W. Since unintentional condensation of either HN_3 or FN_3 in the trap could lead to detonation, the trap was buried in sand inside an aluminum cylinder with 1 in. thick walls, inside a 1/4 in. thick lexan blast shield. The sand was kept dry by a continuous purge of N_2 through the base of the aluminum cylinder. With this arrangement, trap temperatures of -100°C could be maintained for approximately 1 h with a single fill of liquid nitrogen in the dewar.

UV Cell - Absorption cells were inserted in the lines following the HN_3 and FN_3 reactors and the cold trap as diagnostics. The first cell, located after the HN_3 generator was operated at 253.7 nm using a Hg lamp as the source. The intensity of the lamp was attenuated by passage through a pinhole and the lamp supply was driven from a 60 W constant voltage harmonic neutralized transformer to prevent variations in lamp intensity with changes in the line voltage. The probing radiation was directed through a 1/2 in. dia. by 25 cm stainless steel cell (containing the HN_3/He flow) with quartz windows at either end. Opposite the end with the lamp, the probing radiation was detected through a Hg resonance line interference filter by a 1P28 photomultiplier tube. With no HN_3 in the cell, a bias of approximately 750 V generated a steady photocurrent of 100 μa. Under normal operating conditions, the HN_3 in the cell attenuated the probing ultraviolet radiation so that the photocurrent was typically reduced to 25 - 50 μa, depending on the temperature of the HN_3 generator. Based on the known extinction coefficient[12] of HN_3 at 253.7 nm, this result corresponds to an HN_3 yield of 2-4% relative to the flow. This diagnostic provided continuous monitoring of the HN_3 generator that was independent of the other reactions occurring further downstream.

Preliminary experiments tested the operation of the HN_3 generator using a similar absorption cell of commercial design with a D_2 lamp source. Initially, the generator was charged with 2.0 moles of stearic acid (approximately half the volume of the reaction kettle) and 0.5 moles of NaN_3. As shown in Fig. 4, application of constant heater power (by a Variac) produced an exponential approach to a constant temperature over several hours. At the same time, the yield of HN_3 (as measured by absorption) was found to initially increase with the rising temperature and then fall off as the NaN_3 was reacted to completion. The flow rate of gas through the reactor was controlled by a downstream metering valve which exhausted to a vacuum. Therefore, since the generator pressure was regulated, the total gas flow through the metering valve was constant. Consequently, as HN_3 gas was evolved, less He flow was required to maintain the pressure in the reactor. The generation rate of the HN_3 could therefore be monitored by the change of He flow through the mass flowmeter as well. Unfortunately, as the absorption signal began to drop at long times, the change in He flow continued to increase demonstrating that a gas other than HN_3 was also being produced in the reaction kettle. It was theorized that the gas was CO_2 resulting from second order reactions of the sodium stearate produced in the melt as a by-product of HN_3. To test this hypothesis, the experiment was repeated with the NaN_3 charge reduced to 0.1 mole, to reduce the concentration of sodium stearate that was built up. The flow rates of the He carrier gas were adjusted in the two experiments to give approximately the same HN_3/He ratio in either case so that the HN_3 yield could be measured by the same absorption diagnostic. As shown in Fig. 5, reducing the NaN_3 mole fraction had the intended effect. Therefore, the reduced NaN_3 charge was used in all subsequent experiments.

IR Cell - Following the FN_3 generator, the gas was passed through an infrared absorption cell. The function of this cell was to detect residual HN_3 without being affected by FN_3 or HF that might also be present. Haller[1] found that excess F_2 reacted slowly with FN_3 to yield NF_3 and N_2. Consequently, the FN_3 yield peaks when the HN_3 and F_2 flows are titrated. Also, it was undesirable to condense residual HN_3 in the cold trap. Therefore, a residual HN_3 diagnostic was required. The 3.0 μm infrared wavelength was selected for this diagnostic on the basis of the known infrared spectra of FN_3, HF and HN_3, since none of these gases absorb at visible wavelengths, except FN_3, and at ultraviolet wavelengths HN_3 and FN_3 are indistinguishable.[3,6,13]

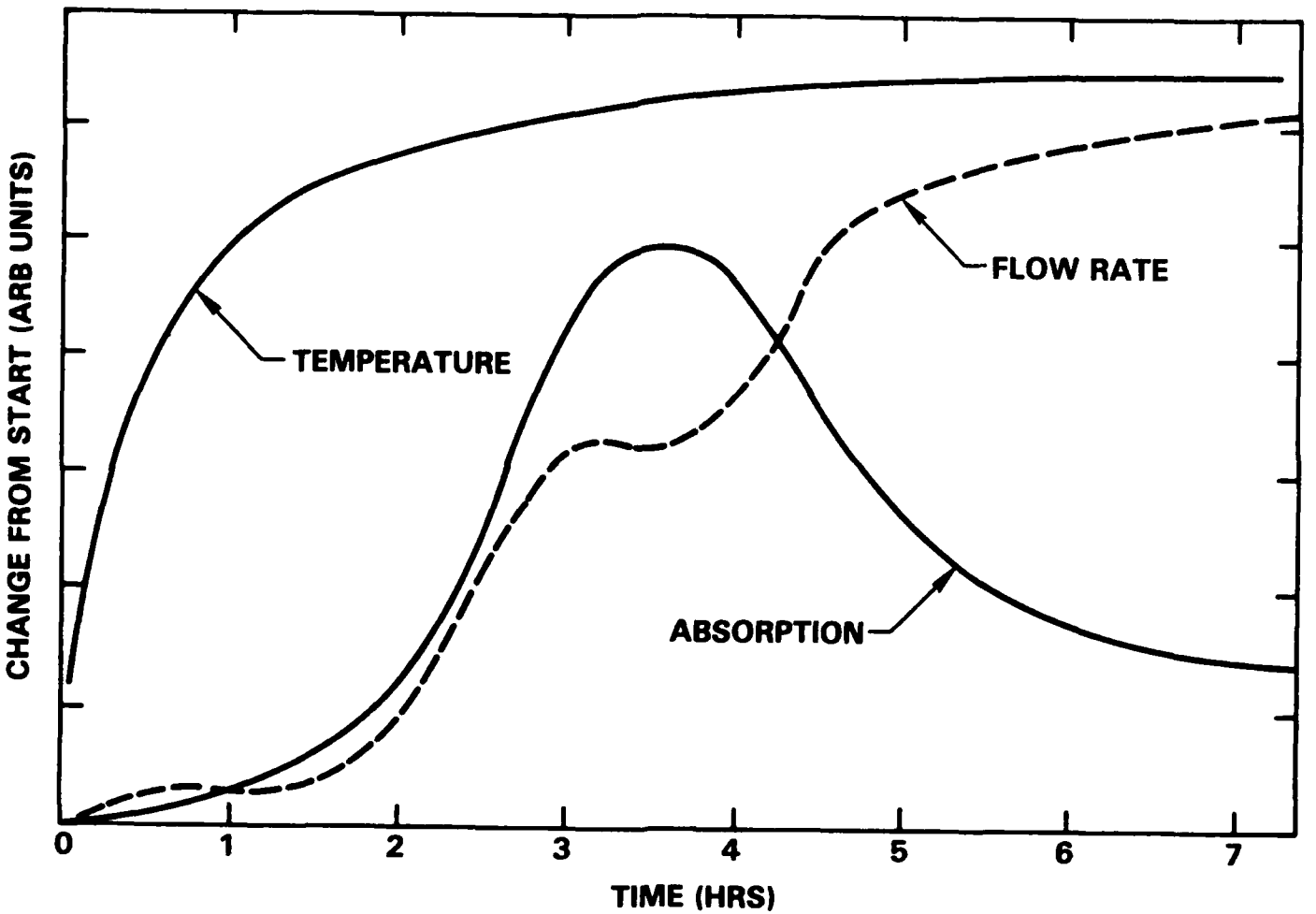

Fig. 4 Temporal behavior of HN_3 generator with constant heater power and 0.5 moles NaN_3 with 2.0 moles stearic acid.

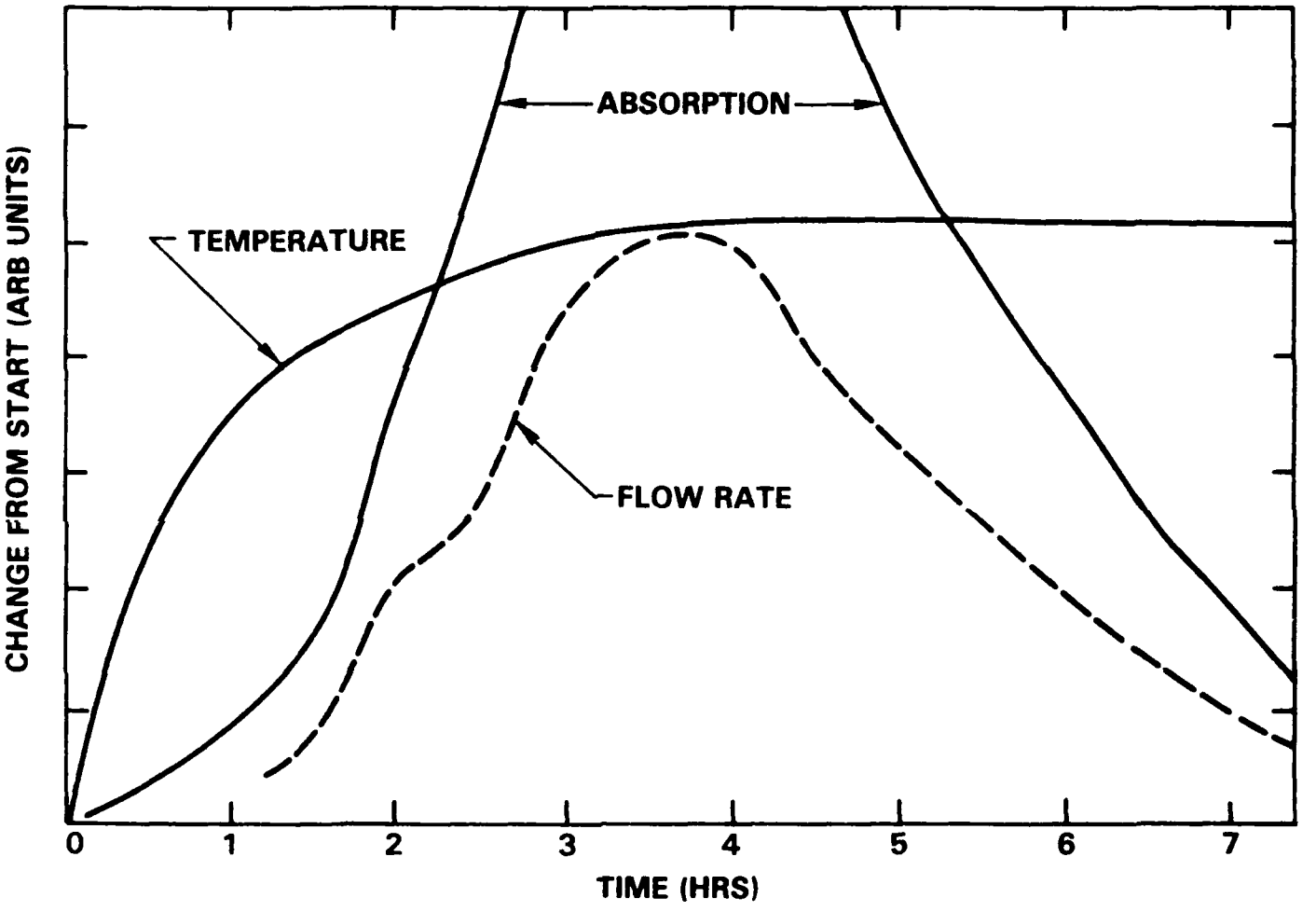

Fig. 5 Temporal behavior of HN_3 generator with constant heater power and 0.1 moles NaN_3 with 2.0 moles stearic acid.

The infrared diagnostic, shown in Fig. 6, was constructed of a 19 mm O.D. × 100 cm long Suprasil quartz tube with sapphire windows at either end. The radiation source was a 900°C (temperature regulated) blackbody with a 3 mm dia. aperture. A 1 KHz mechanical chopper was interposed between the blackbody and the entrance to the absorption cell. At the opposite end of the cell, the radiation was analyzed by an interference filter (60 nm FWHM) and detected by a room temperature 0.4 × 0.4 cm^2 PbSe chip located inside an aluminum box. The detector was biased at 75 V and the photocurrents were passed to a lock-in amplifier via a 2 pole R-C bandpass filter to limit out of band noise. The lock-in amplifier was referenced to the chopper and typically 100 μV signals were recovered to S/N ≥ 10 with 10 s of integration.

The amplitudes of the detected signals, however, were found to be sensitive to variations in the temperature of the detector chip. It was therefore necessary to stabilize the temperature of the detector. A copper plate carrying a resistive heater, a temperature sensing element and a small expansion nozzle was fit to the back of the aluminum box which surrounded the detector and the entire detector box was encased by fiberglass insulation. Application of 60 psig CO_2 to the nozzle produced a steady cooling action which was counteracted by the heating of the resistor. The feedback circuit shown in Fig. 7 was then employed to adjust the resistor current so that the temperature sensor was held at a constant level. The circuit was adjusted to balance at close to room temperature and the test point was monitored with a voltmeter to check the feedback stability. From the amplitude and the frequency of the stable oscillation of the test point about its mean value, it was possible to calculate that the temperature variation at the sensor was less than ± 0.1°C. Application of the temperature stabilizing circuit cured the drifts in the measurement that were caused by the variations of the room temperature.

The infrared diagnostic was tested by operating it in series with a commercial ultraviolet absorption cell (D_2 lamp) and the HN_3 generator; the results are shown in Fig. 8. Clearly, the infrared and ultraviolet diagnostics track the same species, but while the infrared diagnostic is noisier, it shows less baseline drift than does the measurement at the ultraviolet wavelength. The baseline drift of the ultraviolet measurement was traced to adsorption of HN_3 on the cell widnows which typically would recover under vacuum overnight.

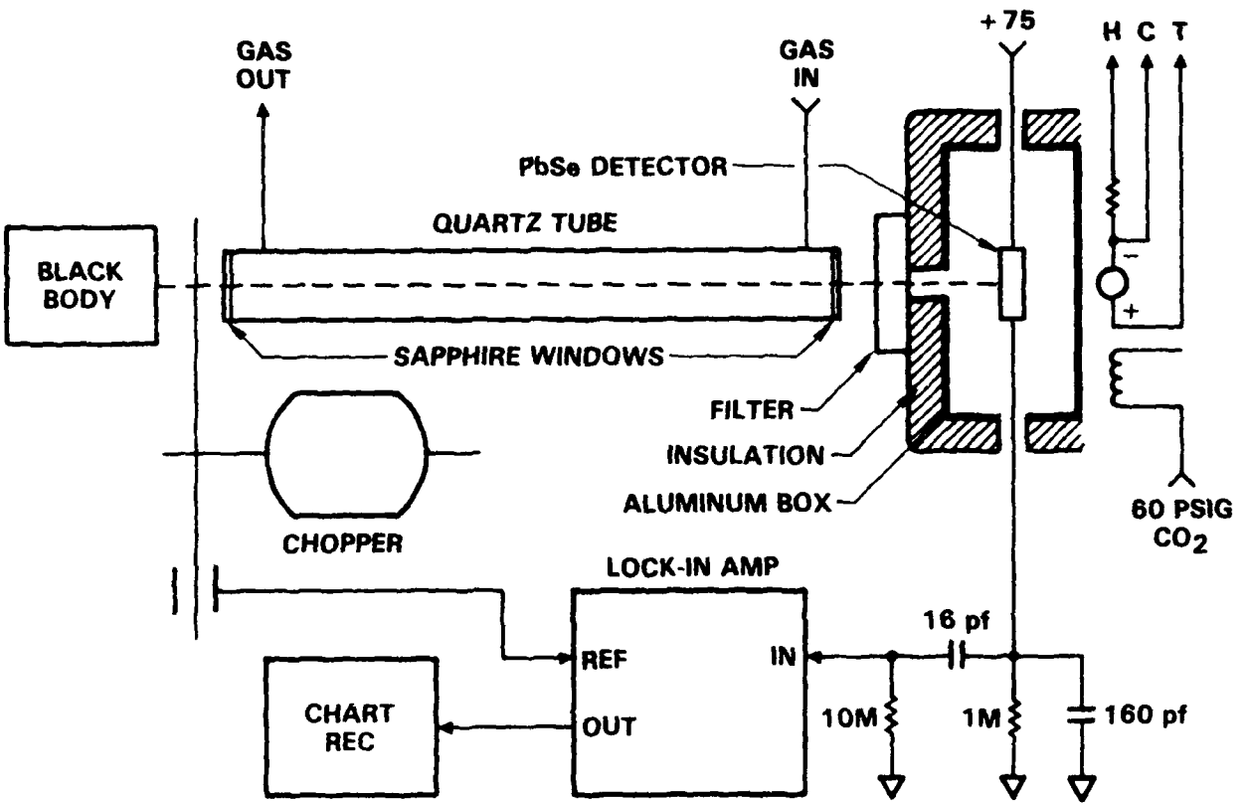

Fig. 6 Schematic of infrared absorption diagnostic.

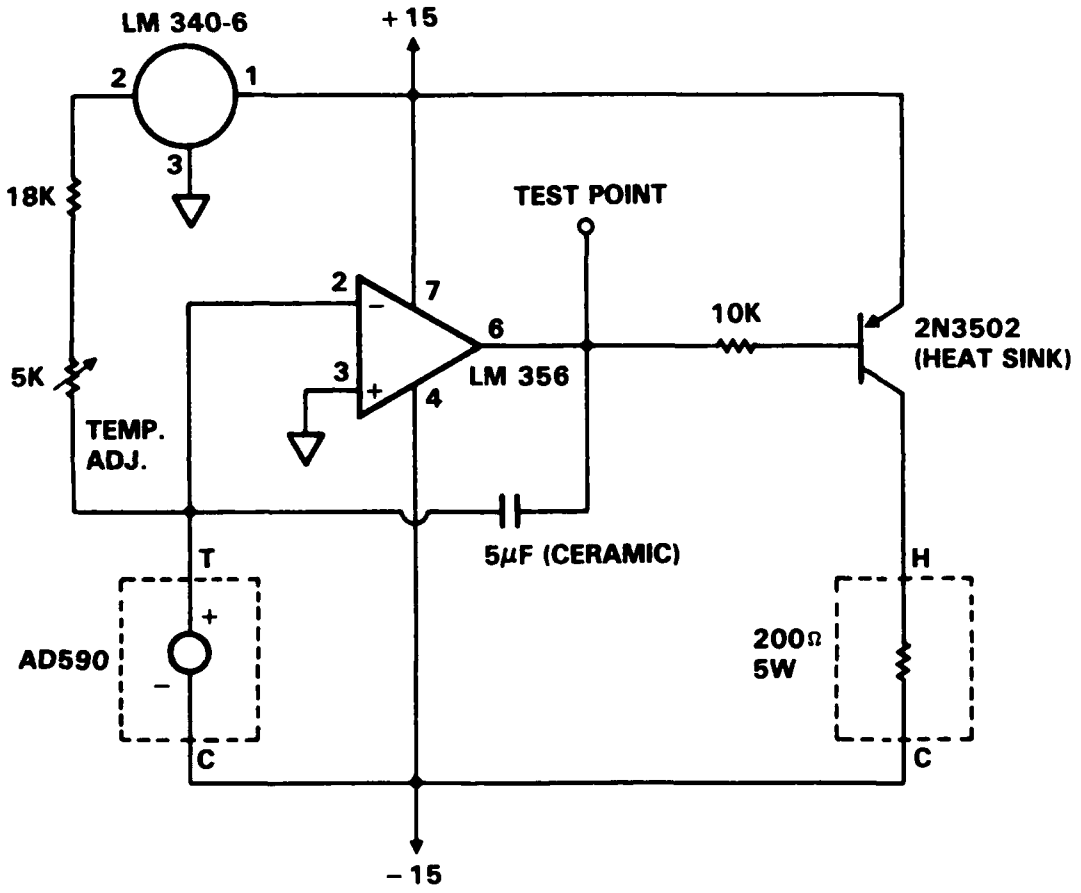

Fig. 7 Feedback circuit for temperature stabilization of PbSe detector.

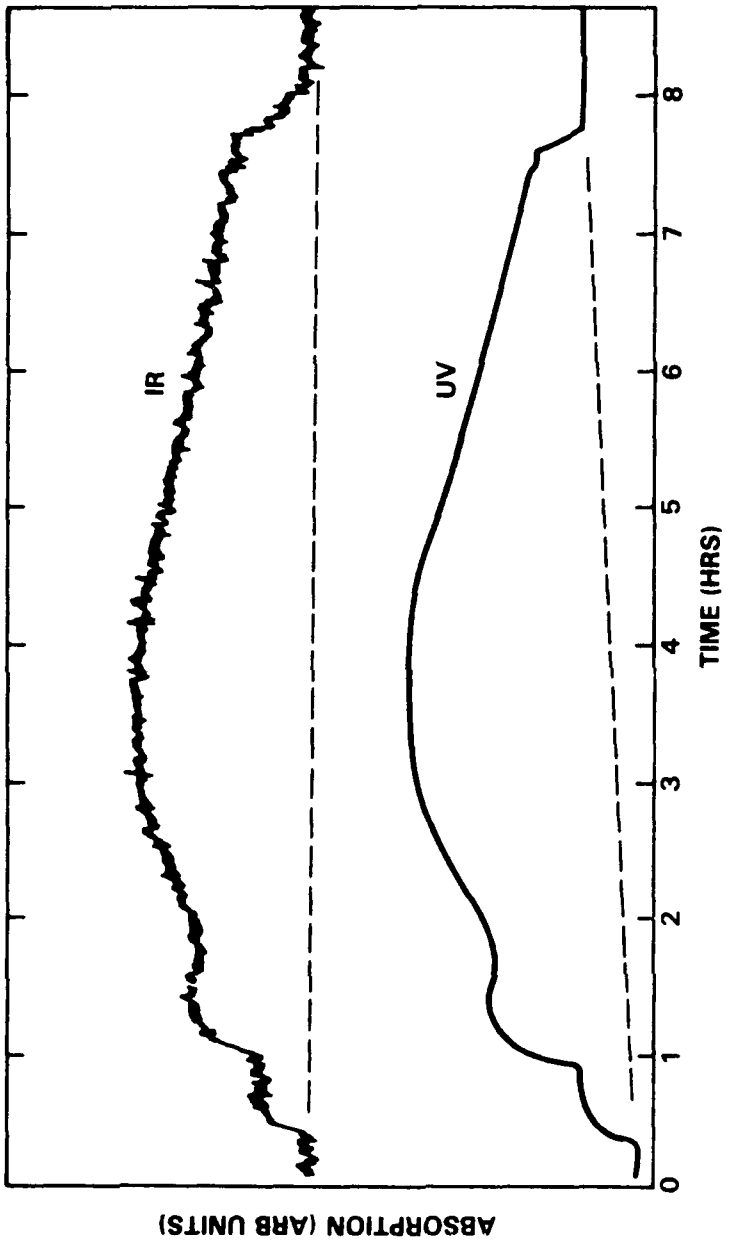

Fig. 8 Comparison of infrared and ultraviolet absorption diagnostics with constant heater power.

Programmed Power Supply - The time profiles of the HN_3 yield shown in Figs. 4, 5 and 8 were still problematical with respect to variation of the yield during the course of the experiments, since continuous adjustment of the F_2 flow was required to maintain an optimal titration with the HN_3 flow. Therefore, the circuit shown in Fig. 9 was employed to program the power to the oil bath of the HN_3 generator in such a way as to counteract the variation of the HN_3 yield. The circuit operates by switching the heater on and off and by slowly varying the duty cycle. The circuit is designed to operate at full power, a constant reduced power and at a power level that linearly increases with time according to the selector switch. Initially, the power is set to full until the oil bath reaches a specified temperature (~ 160°C) and then the circuit is switched to reduced power for typically 3 h. During this time, the temperature falls to a constant level near 100°C and the HN_3 generation rate builds up in a rather complicated, but nonetheless reproducible manner, due to the melting of the stearic acid. Following this, the HN_3 yield would begin a slow linear decline if the power was held constant. Instead, the supply circuit is switched to ramp the power linearly with time over the next 4 h. The increasing temperature accelerates the generation of HN_3 with time, resulting in the near constant HN_3 yield that is evident in Fig. 10 from 4 - 7 h into the run.

The internal controls of the power supply must, of course, be adjusted to produce the temperature vs time curve that is shown in Fig. 10 to achieve the desired result. The adjustments are as follows: (1) controls the cycle rate and should be set for a 60 s cycle period; (2) controls the continuity of the transition from low power to ramped power; (3) controls the low power setting; and (4) controls the amplitude of the ramp. These controls can be set relatively quickly by trial and error using a voltmeter to measure the control voltages and linear extraoplation to predict the desired result from two or more runs. Once set, the stabilized production of HN_3 is quite reproducible if sufficient care is given to precise loading of the generator, the initial heating peak and the time of switchover to ramped power. The use of high heat at early times accelerates the melting of the stearic acid and has a profound effect on the HN_3 time profile thereafter.

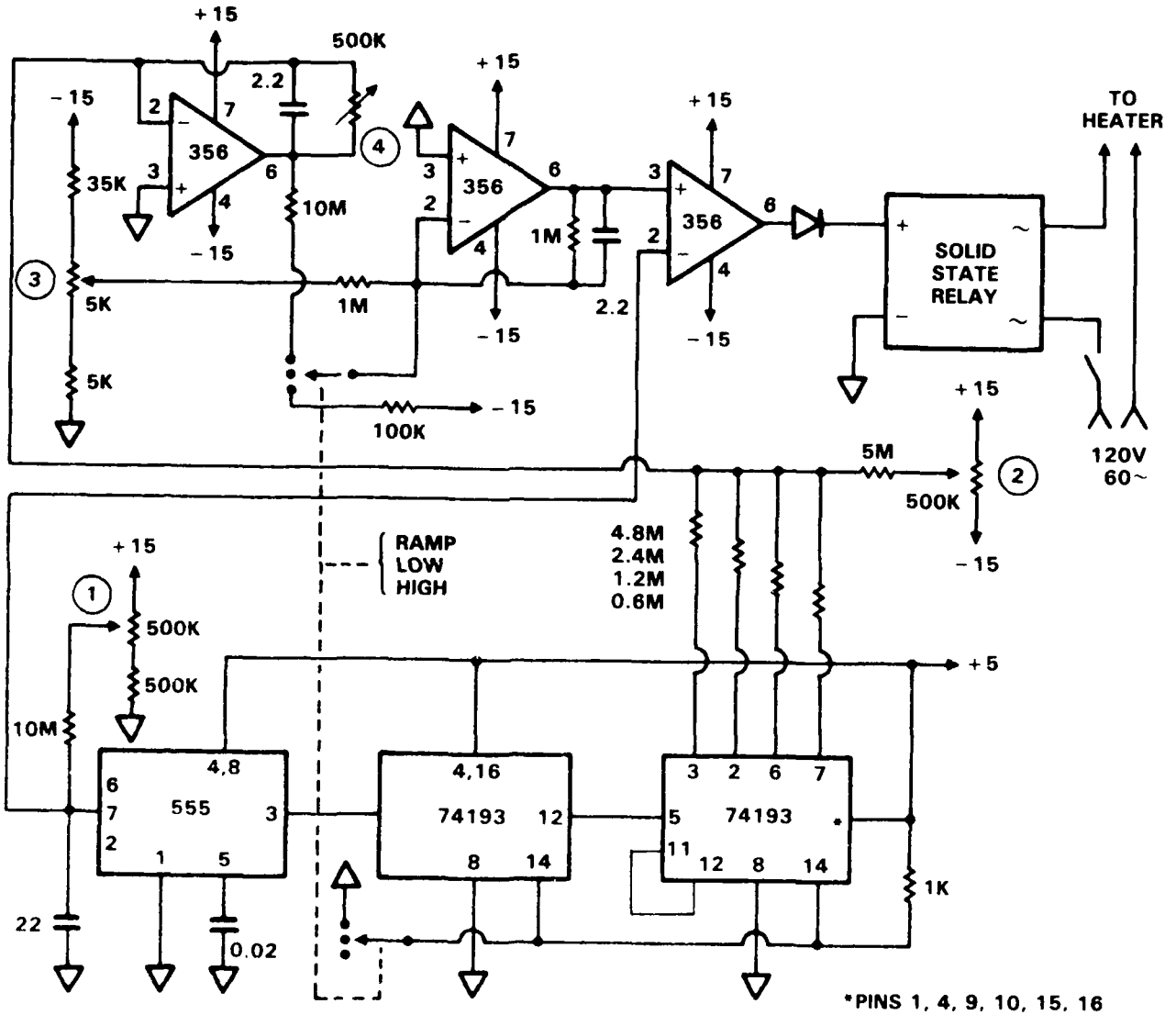

Fig. 9 Schematic of programmed power supply used to stabilize HN_3 generation rate.

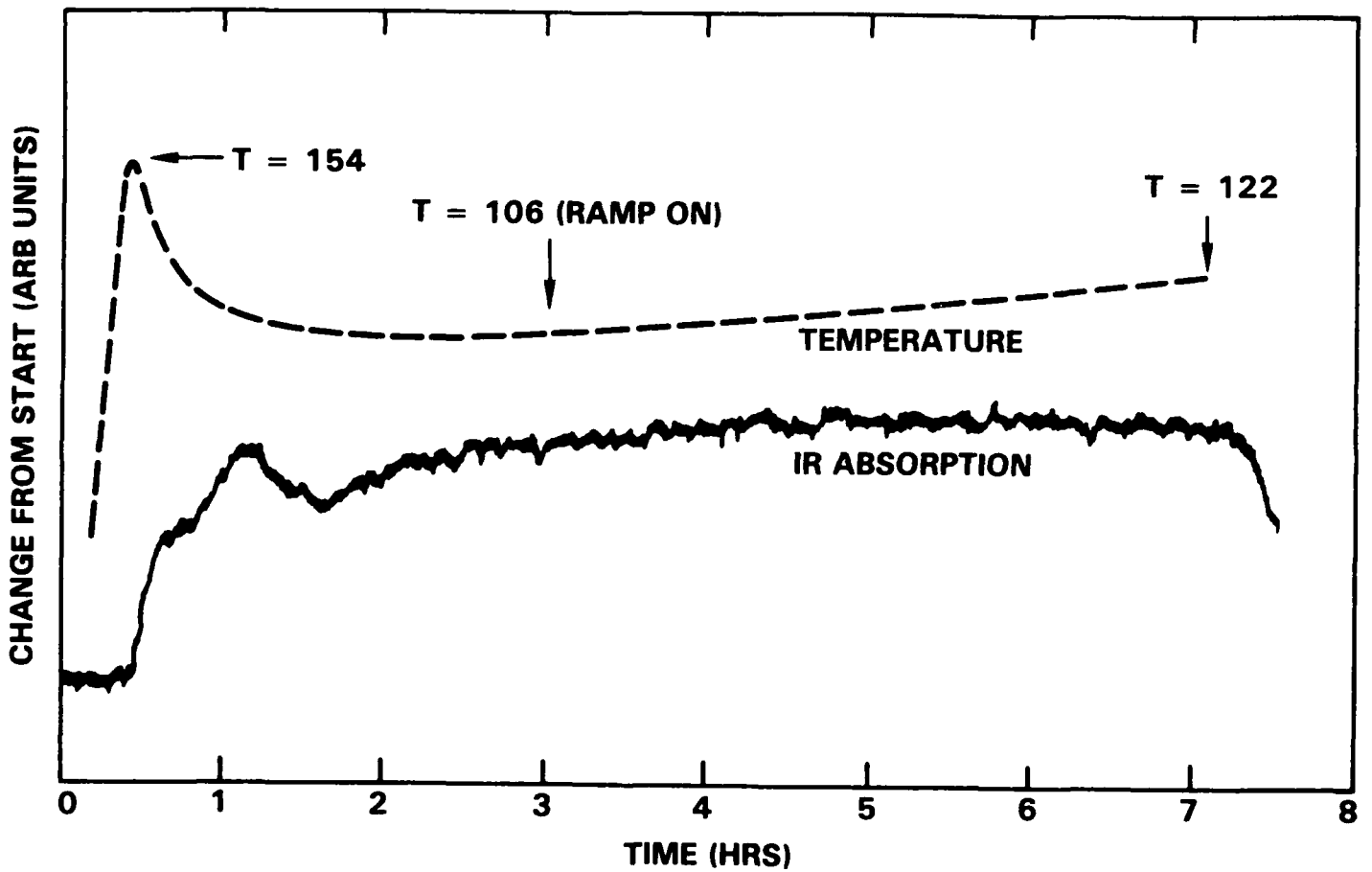

Fig. 10 Temporal behavior of HN_3 generator using programmed power supply.

As a safety measure to prevent prolonged heating at high power, the automatic temperature control on the electric pot is set at 200°C. Normally, since the pot will always be cooler, this control will be inactive (always on). If, on the other hand, the temperature reaches 200°C, the control unit will begin to cycle on and off, thereby preventing any further rise in temperature. The control unit therefore provides an added degree of protection against thermally-induced NaN_3 decomposition[14] which starts at about 250°C.

Once the HN_3 yield was stabilized, it was then possible to test the infrared absorption diagnostic during FN_3 generation. In Fig. 11, the HN_3 yield is first stabilized, then F_2 is added in sufficient quantity to react all of the HN_3. The complete disappearance of absorption shows that the infrared diagnostic is insensitive to F_2, FN_3 and HF, and that there is no baseline drift associated with production of FN_3 since full recovery of the HN_3 absorption occurs once the F_2 flow is shut off. Therefore, the infrared diagnostic can be reliably used as an on-line monitor of residual HN_3.

VIS/UV Cell - Finally, after the trap, the gas stream is passed to a 6 cm stainless steel cell with quartz windows inside a commercial spectrophotometer[15] operated at 420 nm with a tungsten lamp source. At this wavelength, FN_3 can be detected without interference from HF or HN_3.[3,6,12] By systematically varying the F_2 flow, it was found that the FN_3 yield peaked at a slightly lower F_2 flow than was required to eliminate the residual HN_3 entirely (as measured by the infrared absorption diagnostic). During a typical stabilized run, the 420 nm cell transmission decreased from 100 to 92 - 94%, when the FN_3 was generated. Using Gholivand's data for the extinction coefficient[3] of FN_3 indicates that the HN_3 was converted to FN_3 with 50 - 100% efficiency, yielding typically 7 torr of FN_3 in 350 torr of He buffer gas. The metering valve which controlled the system flow rate was located just downstream of the 420 nm absorption cell. From here, the FN_3/He gas stream was conducted to the experiment and exhausted to vacuum by 1/4 in. dia. stainless steel and teflon lines. A pressure gauge just upstream of the metering valve showed little pressure difference between the visible wavelength absorption cell and the vacuum regulator just upstream of the HN_3 generator.

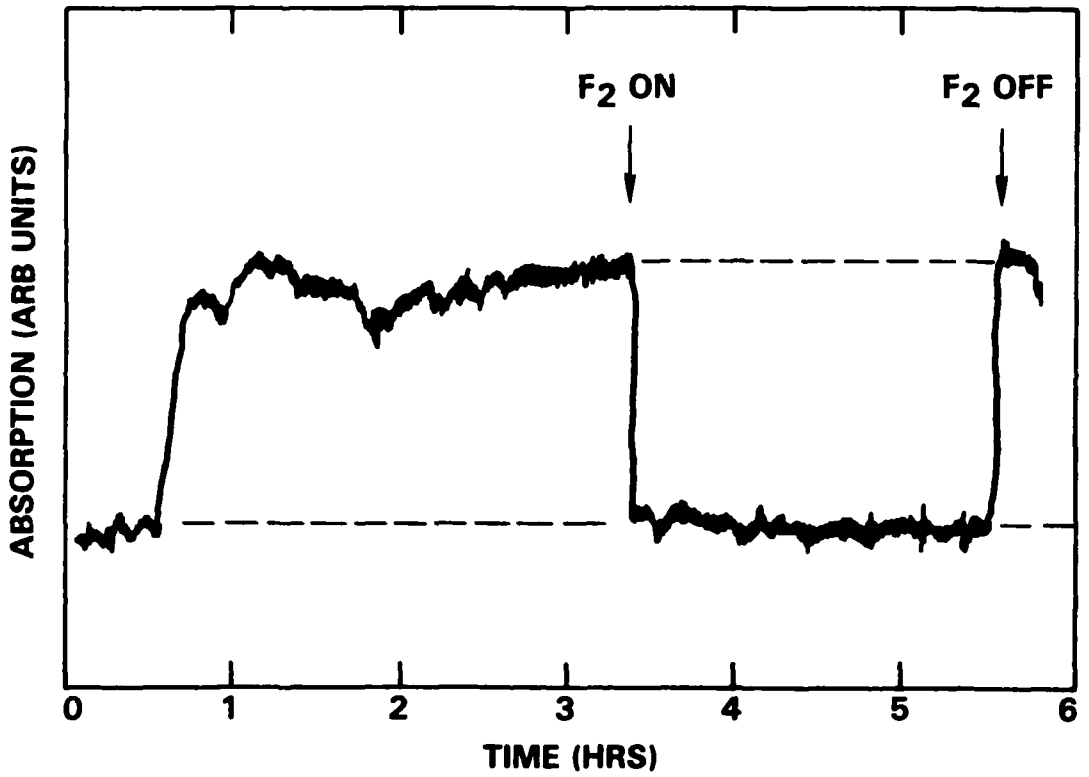

Fig. 11 Response of infrared absorption diagnostic to generation of FN_3.

Miscellaneous - Several additional features of the FN_3 source, not shown in Fig. 2 for reasons of clarity, are discussed below. Some of these have significant safety consequences. Large area course glass frits were placed in the gas lines at the exit of the HN_3 and FN_3 generators. The funtion of these filters is to stop entrainment of particulates from the two reactors by the gas stream. A frit is required downstream of the FN_3 reactor because solid NH_4F can be formed under some conditions as noted by Haller.[1] We strongly recommend that the meter which monitors the output voltage of the mass flowmeter be alarmed to provided an audible warning if the He flow either stops or falls below a preset level, typically half of the nominal flow rate. This is necessary because a vacuum pump failure or clogged valve downstream can stop the He flow resulting in a buildup of high pressures of HN_3 or FN_3 at the generator, intermediate reactor, or trap, resulting in potential for explosion. The stainless steel balls in the intermediate reactor should be checked for signs of corrosion or reaction at regular intervals to prevent buildup of metal azides. Periodic checks at 3-month intervals in our apparatus (with daily runs) showed only trace contamination by NH_4F. Three-way valves and bypass lines were installed to pass the gas stream around the secondary reactor and trap, to divert the gas stream from the trap exit directly to vacuum and to substitute pure He for F_2/He mixture at the inlet of the secondary reactor. These additional lines provide options that may be of value if the trap or metering valve clogs, while substituting He for F_2/He during warm up minimizes the perturbation of the HN_3 yield that occurs when F_2 addition displaces the He flow through the HN_3 generator. An air line tied in with the effluent of the liquid nitrogen boiler is also recommended as a method to remotely return the cold trap to room temperature to assure that all of the contents are expelled. Finally, while a small floor pump could provide the needed vacuum, we exhausted all of our azide experiments to a 300 cfm mechanical pump which had its oil changed on a monthly basis. This practice prevents any significant accumulation of organic azides in the pump oil.

Coldfinger Apparatus

Figure 12 shows the transfer and storage system used to mate the continuous flow FN_3 generator to the coldfinger where static films were prepared and detonated. The storage system served to prevent a direct connection which could allow a large

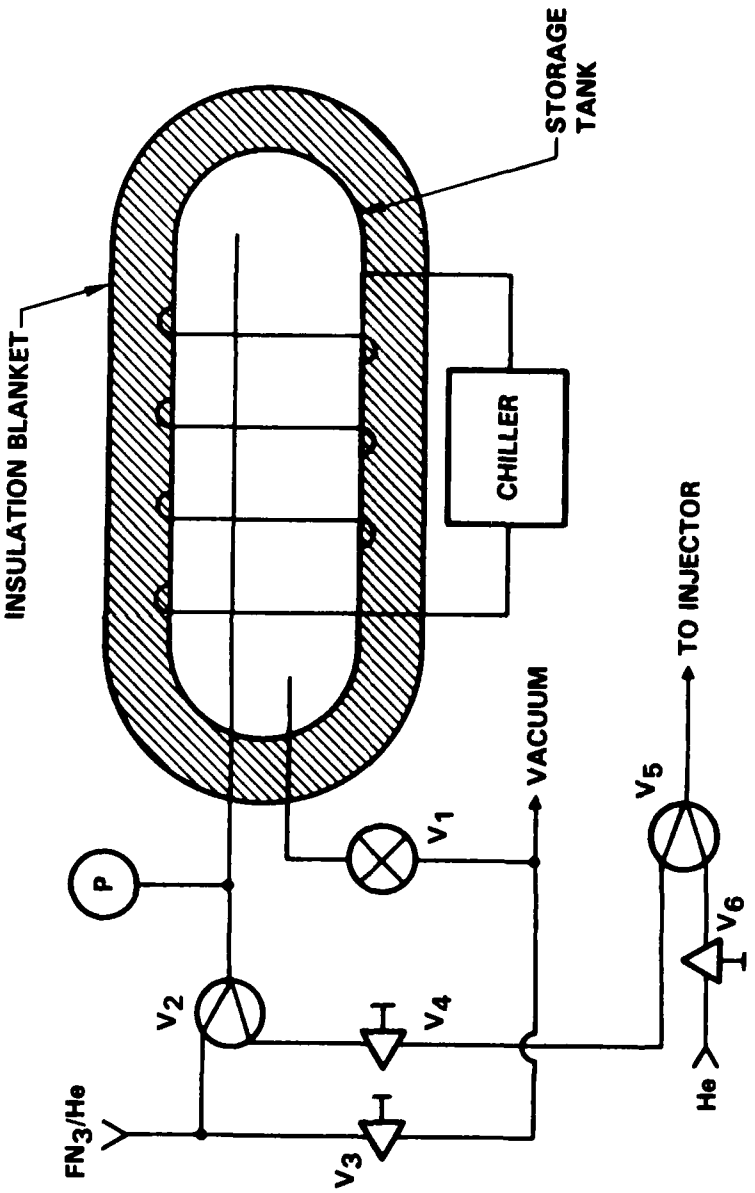

Fig. 12 Schematic of FN_3 transfer and storage system.

quantity of FN_3 to condense in the coldfinger. By charging the coldfinger from the storage tank, it was also possible to use the FN_3 generator on other projects simultaneously with the production and detonation of FN_3 films. A 4 liter stainless steel tank was internally coated with teflon and a cooling coil was brazed on the outside. The tank was wrapped in an insulating blanket and the cooling coil was attached to a closed loop chiller which used a water-ethylene glycol mixture as the coolant. The chiller was set to 0°C and run continuously. Chilling the tank was done because both Haller[1] and Gholivand[3] observed that FN_3 decomposes to N_2F_2 and N_2 slowly in the gas phase at a rate that is strongly influenced by temperature. Even the modest chilling from room temperature to 0°C was expected to increase the lifetime of the FN_3 in the tank from thirty minutes to several hours. In operation, valve (V1) was opened to evacuate the tank and then closed. The three-way valve (V2) was set to attach the tank to the FN_3 line and the bleed valve (V3) was set so that the tank filled to a steady pressure of 100 - 150 torr. The three-way valve (V2) was then switched so that the tank could exhaust via metering valve (V4) and three-way valve (V5) into the coldfinger to deposit the film. The three-way valve (V5) could also be set to admit pure He to the coldfinger through metering valve (V6) instead of the FN_3/He gas from the storage tank. An inductance manometer on the storage tank monitored its pressure. Typically, there was sufficient FN_3/He mixture in the storage tank to make a full day's supply of films.

Detonation Chamber - The coldfinger apparatus itself is shown in Fig. 13. It consisted of a stainless steel, reentrant dewar onto which a copper block was mechanically secured inside the vacuum chamber. The copper block was machined to accept a 1 in. dia. by 1/4 in. thick substrate with a 1/2 in. dia. viewing hole through the center. The substrate was aligned with four O-ring sealed CaF_2 windows around the perifery of the chamber. Lexan plates were mechanically secured over the windows to protect viewers in the event of accidential damage to the windows. The dewar section was purged with a He flow from the top, where a pressure measurement was also affected by means of a capacitance manometer. Radiation from an incandescent lamp was passed through a 420 nm interference filter and coupled via a focusing lens to a short, ultraviolet grade fiber optic bundle which terminated into a telescope and collimating lens attached to the window in front of the substrate. Light emanating from the telescope was passed

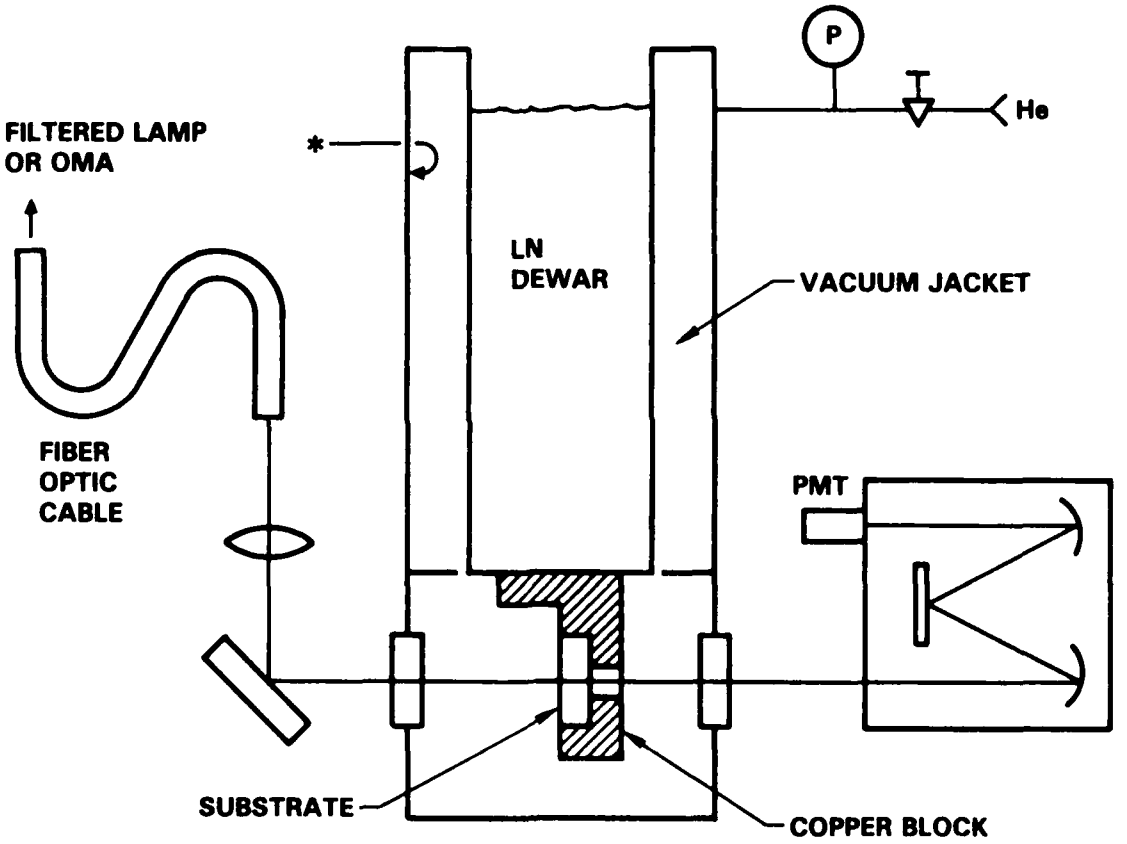

Fig. 13 Coldfinger apparatus for production of FN_3 films.

through the substrate out of the opposing window and through a lens to the entrance slit on a grating monochromator fitted with a GaAs photomultiplier tube. The resulting anode currents, monitored by a picoammeter, served as a useful diagnostic for the presence of a FN_3 film on the substrate. Based on Gholivand's gas phase data,[3] a 50% absorption corresponds to a film of 5 - 10 μm thickness. Alternatively, the end of the fiber optic bundle that was attached to the lamp could be rerouted to the entrance slit of a 0.1 meter monochromator and optical multichannel analyzer (OMA) to capture the emission spectrum resulting from detonation of the film.

Several features not shown in Fig. 13 (for clarity) are shown in Fig. 14, which is an end-on view of the detonation chamber. The films were produced by spraying the FN_3/He gas mixture into the cell through the injector above and to the left of the substrate. The injector was a teflon-jacketed, stainless-steel tube with a 1/4 in. dia. stainless-steel ball on its tip with a 0.013 in. dia. hole through which the gas escaped. The function of the teflon liner was to act as an electrical insulator so that the injector could also be used as a discharge electrode to generate a plasma inside the detonation chamber for cleaning of the substrates. During cleaning, pure He was admitted through the injector to a pressure of 0.5 torr and the discharge was supported by current drawn from a miniature neon sign (constant current) transformer with a secondary rating of 3000 V at 18 ma. The use of the ball on the tip of the injector prevented formation of hot spots in the discharge and the volume in the detonation chamber was filled with a diffuse blue glow. Cleaning was typically done for 10 min with the substrate chilled to near-liquid nitrogen temperature. Other ports on the detonation chamber (located between the CaF_2 windows) were used for pumping gases off to vacuum, admitting themocouple leads to monitor the temperature of the copper block and admitting the laser beam used to detonate the films.

The laser used to detonate the films was a PRA Model LN-1000 nitrogen laser which produced 1 mj pulses of 337 nm radiation with 0.7 ns FWHM pulse duration. The laser output was conducted to the detonation chamber by four dielectric-coated mirrors, a long focal length lens to counteract beam divergence and a focusing lens which also served as a window. A fast photodiode (PD) was employed to sense the firing of the laser since the laser discharge was triggered by a spark gap that contributed significant jitter in time between the electrical command to fire and the appearance of the laser pulse.

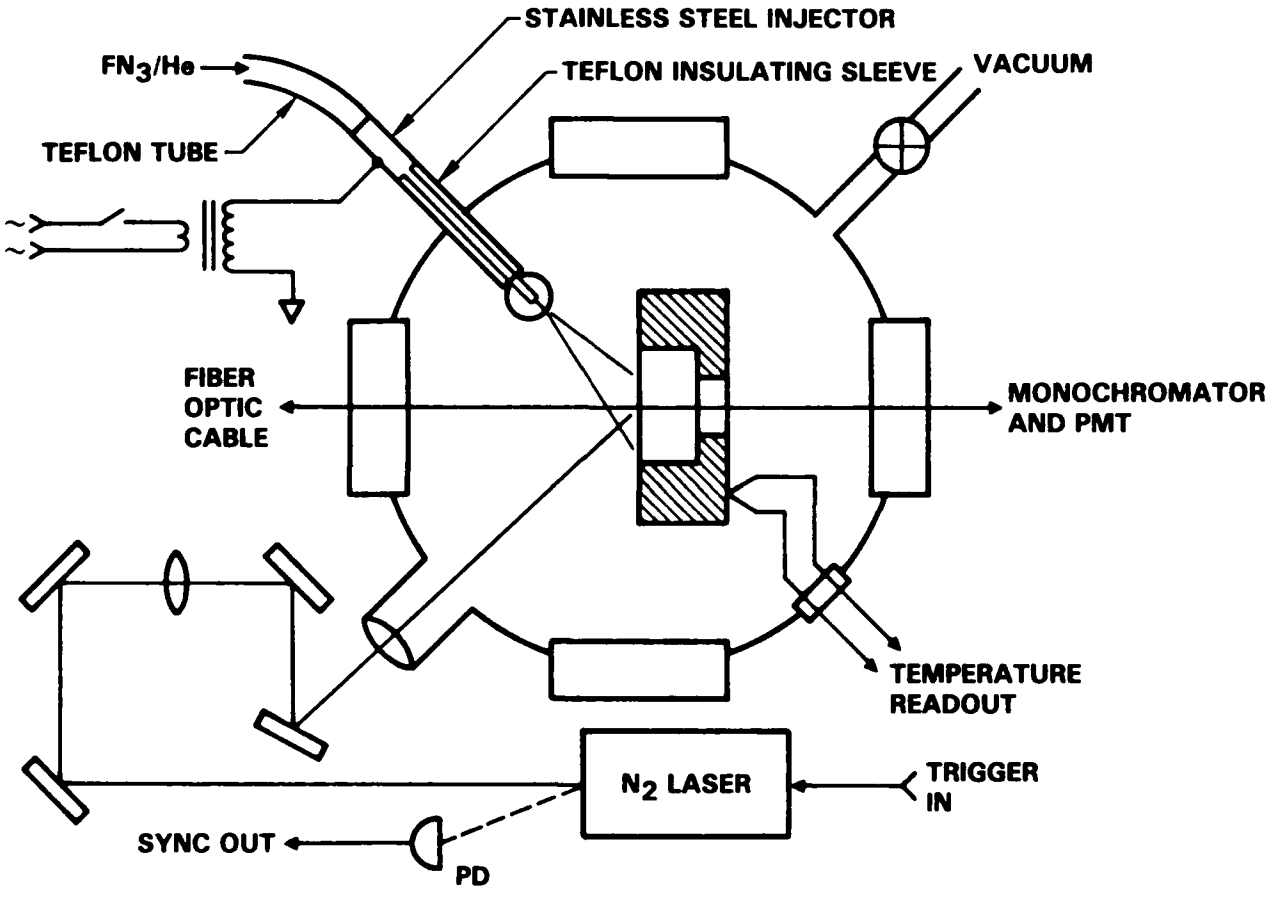

Fig. 14 Cross sectional view of detonation chamber.

Operational Procedure - Production and detonation of films was strongly influenced by several factors, including the substrate temperature, the partial pressure of FN_3 in the chamber, the substrate material, and its surface condition. As Fig. 15 shows, approximately 100 mtorr of FN_3 or 5 torr of 2% FN_3/He mixture is required to support condensation at temperatures achievable with liquid nitrogen as the coolant (typically - 170°C). To achieve this concentration, the pump off line was either closed or restricted at the valve shown in Fig. 14. We found that it was quite difficult to form films on SiO_2 (quartz) substrates if they were not first cleaned via exposure to the He plasma and that films formed somewhat more easily on similar CaF_2 surfaces. Use of plasma cleaning made film deposition quite easy on CaF_2 and gave some improvement on SiO_2. However, the films generated on SiO_2 frequently self-detonated before reaching nominal thickness. Since Haller observed that FN_3 bonds to KF, it is reasonable to expect that a polar surface such as CaF_2 will more easily support a film than SiO_2, which has much greater covalent character. On the plasma-cleaned CaF_2 surfaces, 5 - 10 μm-thick films were formed quite rapidly (within a few seconds) once the critical concentration of FN_3 was added to the detonation cell.

All of the films formed on CaF_2 and SiO_2 substrates were reliably detonated by the nitrogen laser, provided the titration of HN_3 with F_2 was properly balanced in the FN_3 generator. The detonations were readily observable by eye and could be confirmed by the disappearance of absorption at 420 nm following the laser pulse. The operating temperature of the cold trap was selected by producing FN_3 and then reducing the trap temperture until the FN_3 yield at the visible absorption cell began to attenuate at - 105°C, in good agreement with Fig. 15. The trap temperature was then increased slightly to - 95°C to prevent condensation of the FN_3, which could lead to an explosion. At this temperature, the HF by-products and residual HN_3 from the FN_3 generation reaction are two orders of magnitude less volatile[16] than FN_3 and, hence, are very effectively removed from the flow by the cold trap. Use of the cold trap had little effect on our abililty to detonate the films. However, in early experiments without the cold trap and without the infrared absorption diagnostic to guide the titration, films were frequently generated which proved to be quite difficult to detonate by application of a laser pulse. Since residual F_2 or HN_3 can slowly react with FN_3 in the storage tank, this result may simply be the consequence of diluting the FN_3 films with large concentrations

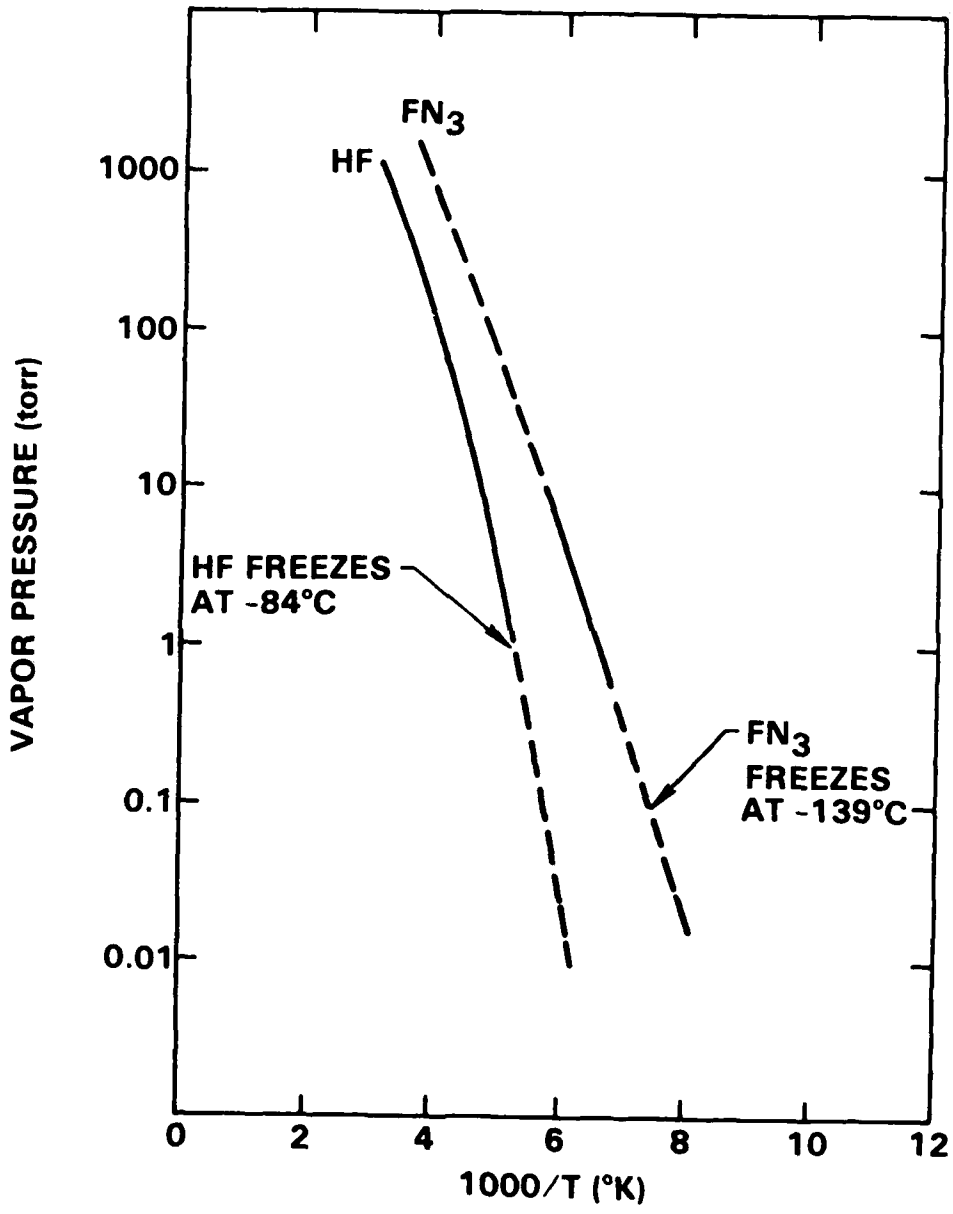

Fig. 15 Vapor pressure curves of FN_3 and HF.

of HF, HN_3 and NF_3 by-products, all of which would condense onto the substrate along with the FN_3.

Detection System

The OMA used to detect the emissions from the FN_3 film detonations was operated on an internal time basis which read and erased the detector array once every 20 ms with a 0.5% duty cycle. Therefore, experiments must begin and end during the first 100 μs after the start of an OMA scan. Figure 16 shows (in block form) how the synchronization and OMA temporal gating functions were achieved. A ready signal (negative transition) from the OMA is applied to the synchronization circuit that is shown in Fig. 17. The voltage at the output of this circuit remains zero until the normally open arm button is first pushed (which lights the LED indicator) and the normally open fire button is pushed. Then, the next OMA ready signal produces a pulse at the output and simultaneously disarms the circuit so that no more pulses are obtained. This single output pulse is used to fire the laser near the start of an OMA scan. The jitter between the command signal and the laser firing is still small compared to the 100 μs aperture time of the OMA. The sync pulse from the fast photodiode is then used to fire a pulse generator which produces a TTL output with variable delay and width. In all of our present experiments, the delay is set to zero and the width to 10 μs. The pulse generator is used to provide a signal to the OMA to cause it to store the data from the detector head in memory at the end of the sweep. Also, the pulse generator output is applied to an amplifier that drives the intensifier section of the OMA which accomplishes the gating function. Accumulated delays in the photodiode, pulse generator, gate driver and the intensifier result in a net 100 ns delay before the OMA begins to accumulate optical data. Following the experiment, the spectral data, stored in memory, are slowly read out to an X-Y chart recorder.

Figure 18 shows the instrument response function of the OMA (not including the fiber optic cable) which was measured using a blackbody source from 475 to 900 nm and an Hg lamp from 300 to 525 nm. The known relative intensities of the Hg lines[17] were converted to absolute intensities by comparison to the blackbody source in the region of spectral overlap. The OMA was fitted with 150 μm slits which yielded 2 nm resolution and approximately a 150 nm range at each setting of the monochromator grating.

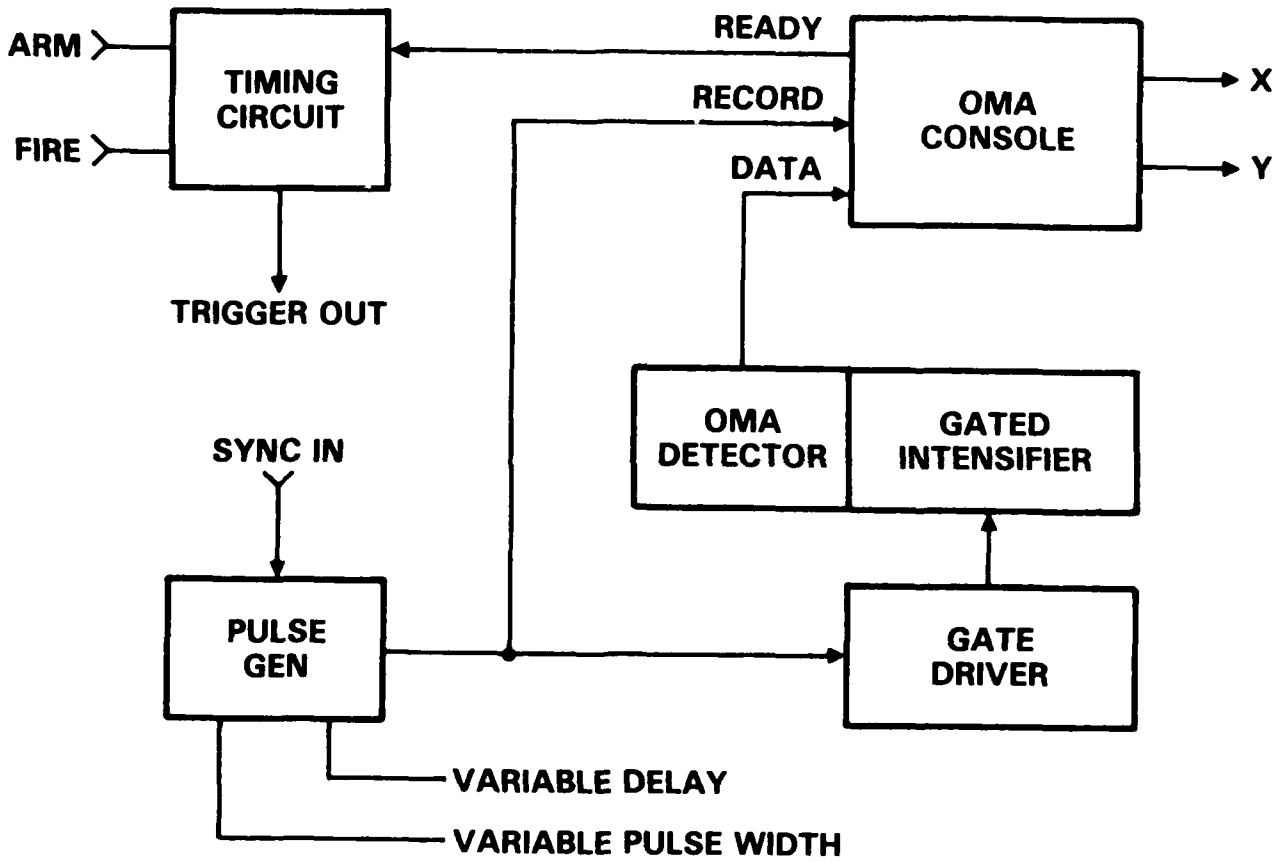

Fig. 16 Block diagram of optical detection system.

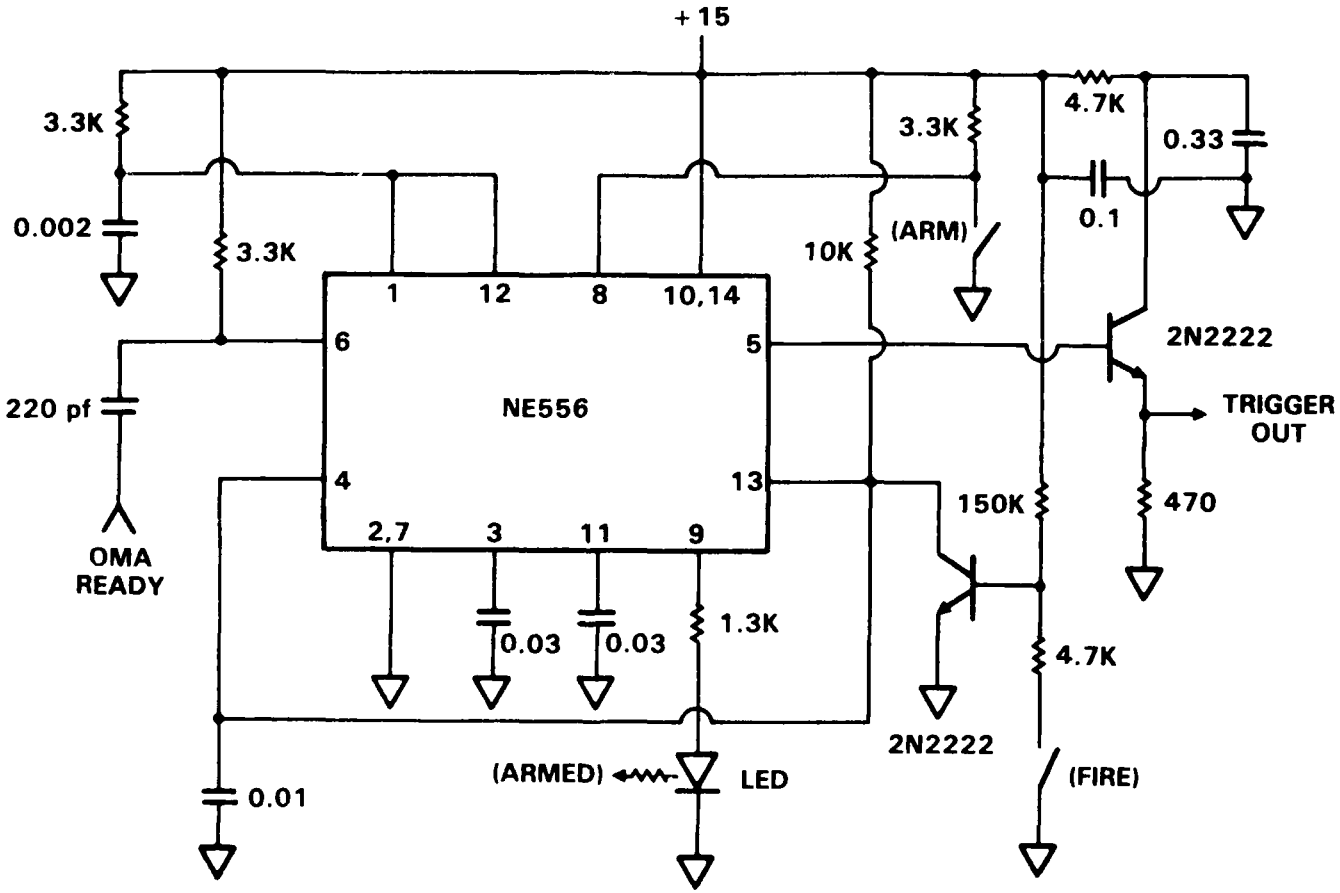

Fig. 17 Schematic diagram of synchronization circuit.

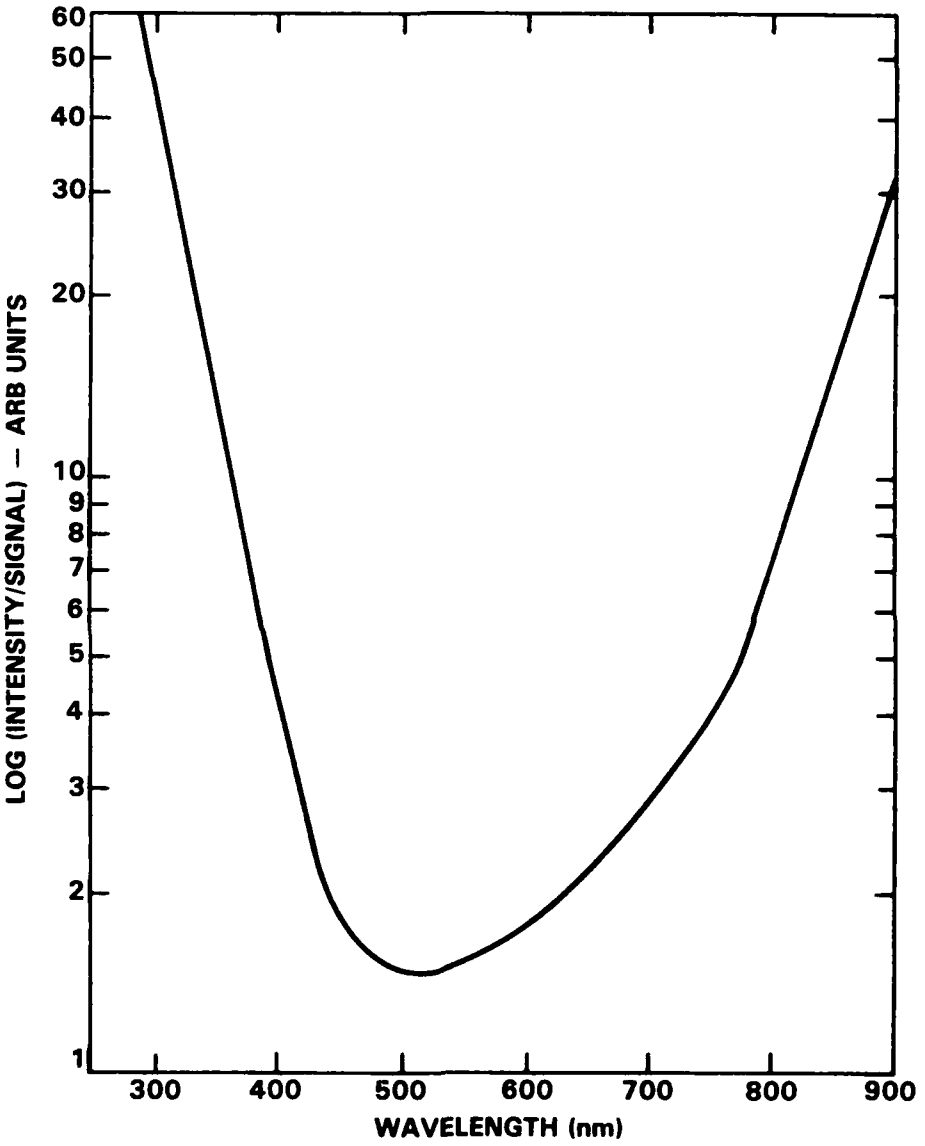

Fig. 18 Instrument response function of OMA and monochromator.

SPECTROSCOPIC RESULTS (PHASE I)

In this section, we will present only those results that were obtained with the full complement of instrumentation just described. Results obtained earlier in the program while the instrumentation was being developed have been deleted.

Impurities

The first issue which needs to be addresed is the extent to which the substrate and any impurity by-products of FN_3 are active in the production of the emissions which occur upon detonation of the films. The key variable with respect to impurity participation is the temperature of the cold trap in the FN_3 generator. Figures 19, 20 and 21 present the emission spectrum from detonations of 5 - 10 μm thick FN_3 films on plasma-cleaned CaF_2 substrates obtained with the cold trap at room temperature. The films therefore contain significant amounts of HF as an impurity since it is a condensible by-product of FN_3 that is generated in equimolar concentration by the reaction of F_2 with HN_3. The films may also contain a small amount of residual HN_3 left over from the same reaction. Figures 22 and 23 present similar emission spectra except that the cold trap was operated at -95°C during the production of the FN_3. Since at this temperature species less volatile than FN_3 will condense in the trap and more volatile species will fail to condense on the coldfinger, the films can be regarded as essentially pure if there are no other sources of contamination. Comparison of Figs. 19 and 22 shows that in the near ultraviolet region, the bands at 337, 360 and 392 nm are independent of impurity concentration, while some of the emissions in the 435 - 465 nm region are attenuated by use of the cold trap. In the visible region (Figs. 20 and 23), there are essentially no differences between the bands with and without the cold trap on-line. Finally, there were no detectable emissions in the near-infrared band, out to 900 nm, from the detonation of cold trap purified FN_3 on CaF_2 substrates. Therefore, the bands which are seen in Fig. 21 are impurity related. From these results, we can conclude that impurities in the gas stream do not contribute to the production of the ultraviolet emissions below 400 nm.

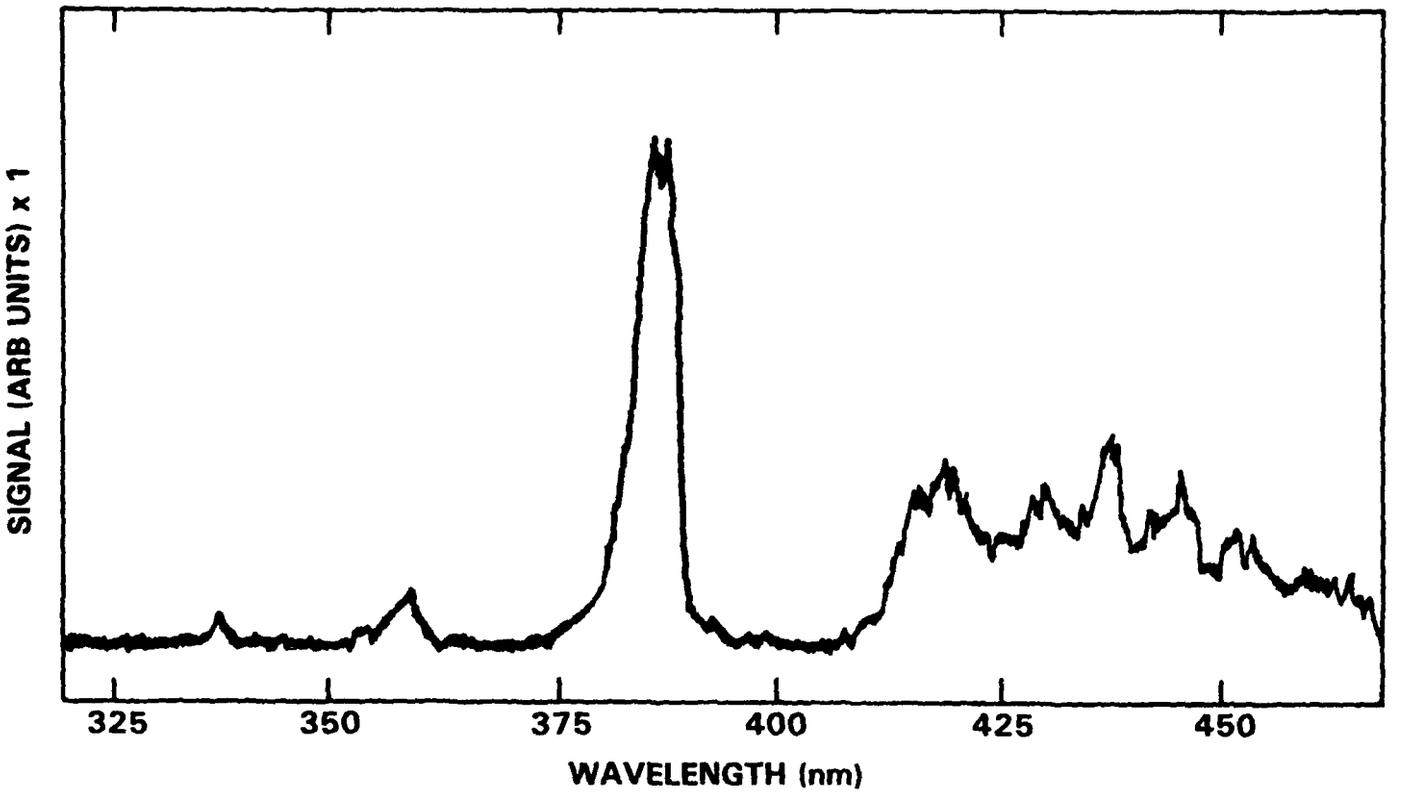

Fig. 19 Near-ultraviolet emission spectrum of FN_3 film detonation on plasma-cleaned CaF_2 substrate.

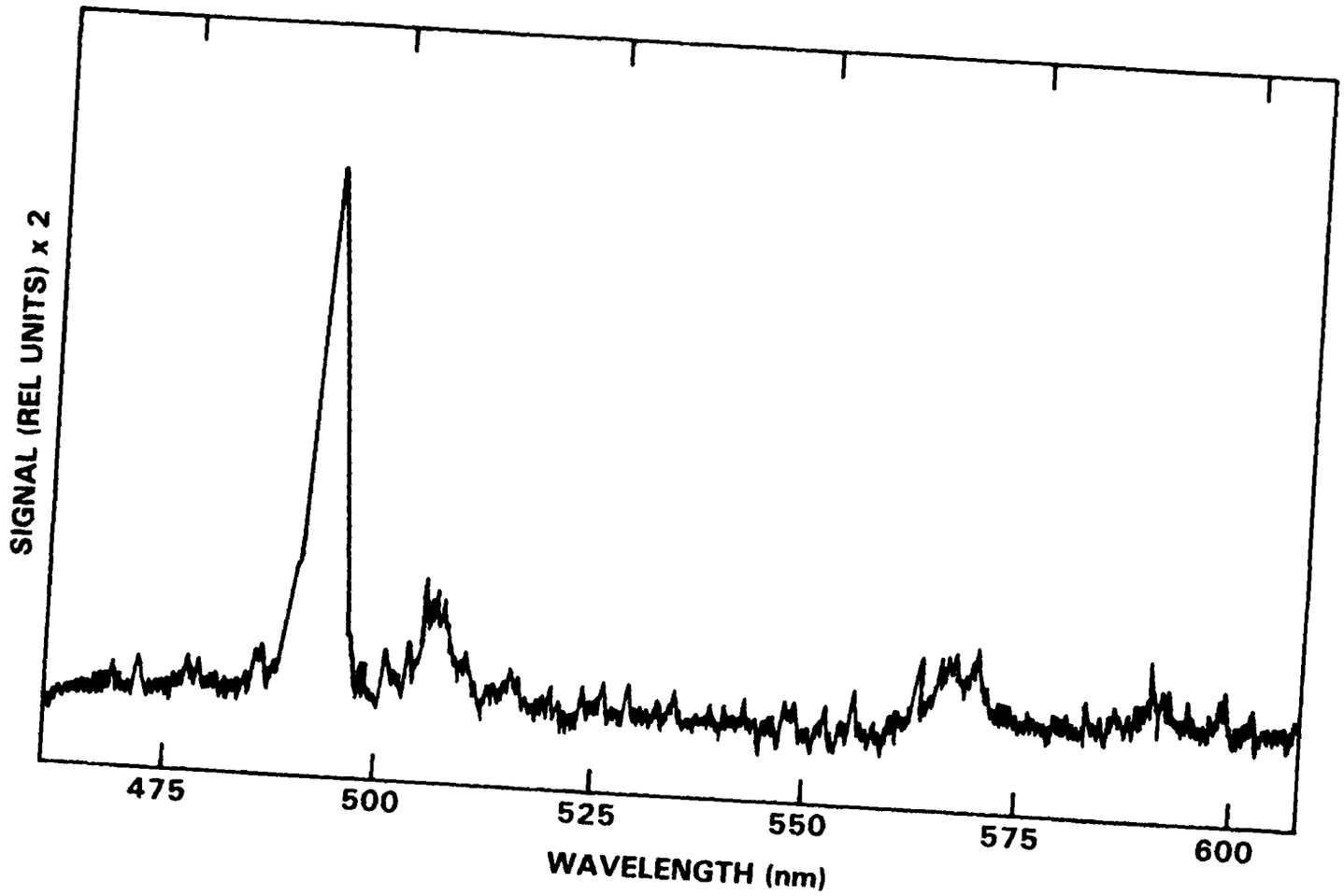

Fig. 20 Visible emission spectrum of FN_3 film detonation on plasma-cleaned CaF_2 substrate.

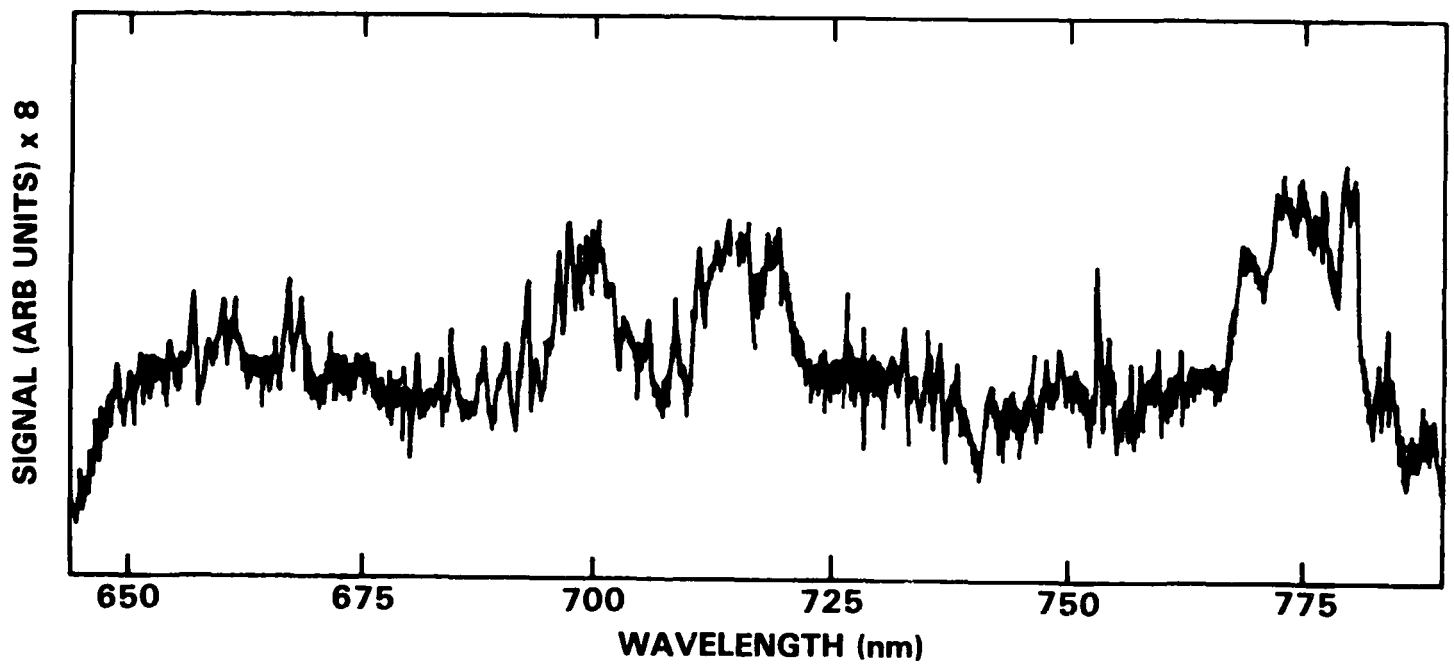

Fig. 21 Near-infrared spectrum of FN_3 film detonation on plasma-clean CaF_2 substrate.

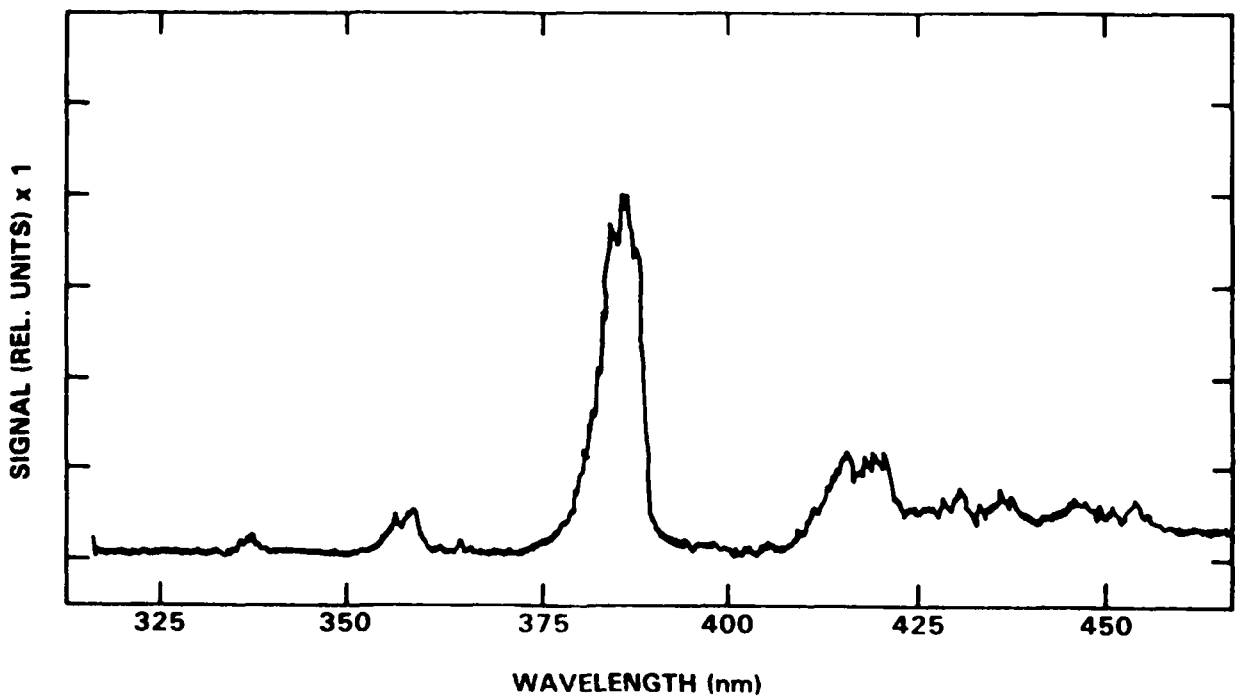

Fig. 22 Near-ultraviolet emission spectrum of cold trap purified FN_3 film detonation on plasma-cleaned CaF_2 substrate.

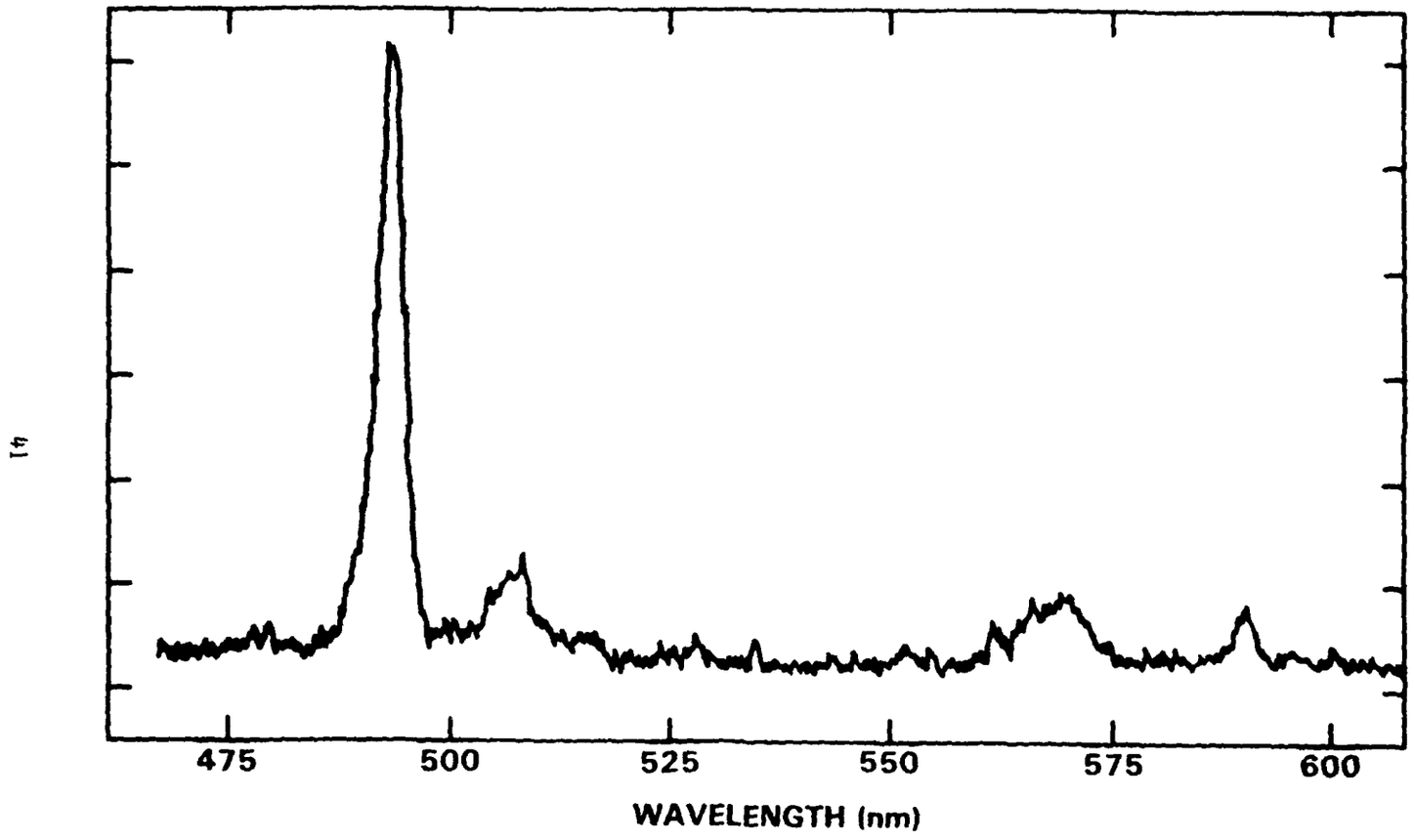

Fig. 23 Visible emission spectrum of cold trap purified FN_3 film detonation on plasma-cleaned CaF_2 substrate.

Figures 24 and 25 present the visible and near ultraviolet emission spectra from FN_3 film detonations on SiO_2 (quartz) substrates. While these detonations were harder to obtain and were from thinner films than on CaF_2, comparison with Figs. 22 and 23 shows that essentially identical emission spectra were obtained except for overall emission intensity. From these results, we can conclude that while the substrate material has a physical role in the formation of the film, there is no chemical participation of the substrate in the detonation process, however, we did find that the CaF_2 substrates were more survivable than quartz. After three to five shots the SiO_2 substrates began to show pitting at the point where the laser beam detonated the film. Detonation of FN_3 films substantially thicker than 5 - 10 μm frequently cracked either substrate within a few shots.

Emitting Species

The second important issue is the assignment of the emission spectrum to the molecular fragments generated by the detonation of the FN_3 films. Based on the discussion in Section 1.0 of this report, one would naturally look for NF(a) and NF(b) as primary products of FN_3 decomposition. No NF(a → X) emission was observed at 874 nm which is understandable, since NF(a) has a radiative lifetime of 5.6 s[18] and therefore only two out of every million NF(a) molecules can radiate within the 10 μs aperture time used in our experiments. Taking this factor and the known sensitivity of our diagnostic[19] into account, it is a marginal proposition at best to see any NF(a → X) emission even if every FN_3 molecule in the film is efficiently converted to NF(a).

The radiative lifetime[20] of NF(b), approximately 20 ms, is much shorter than that of NF(a). Detection of NF(b → X) emission is therefore feasible, which in most sources appears as a narrow band at 528 nm. The Franck-Condon factors of the NF(b → X) transition[21] tend to restrict the emission to the $\Delta v = 0$ sequence since the molecule has highly vertical potential energy curves. The usual chemiluminescent sources of NF(b), such as the $F + HN_3$ flame,[22] are typically characterized by low vibrational temperatures, thus only the $v' = 0$ to $v'' = 0$ transistion is significant in these cases. It is also a characteristic of these sources that the pressure of He buffer gas is around 1 torr, which is sufficient to thermalize the vibrational ladder of the NF(b) state

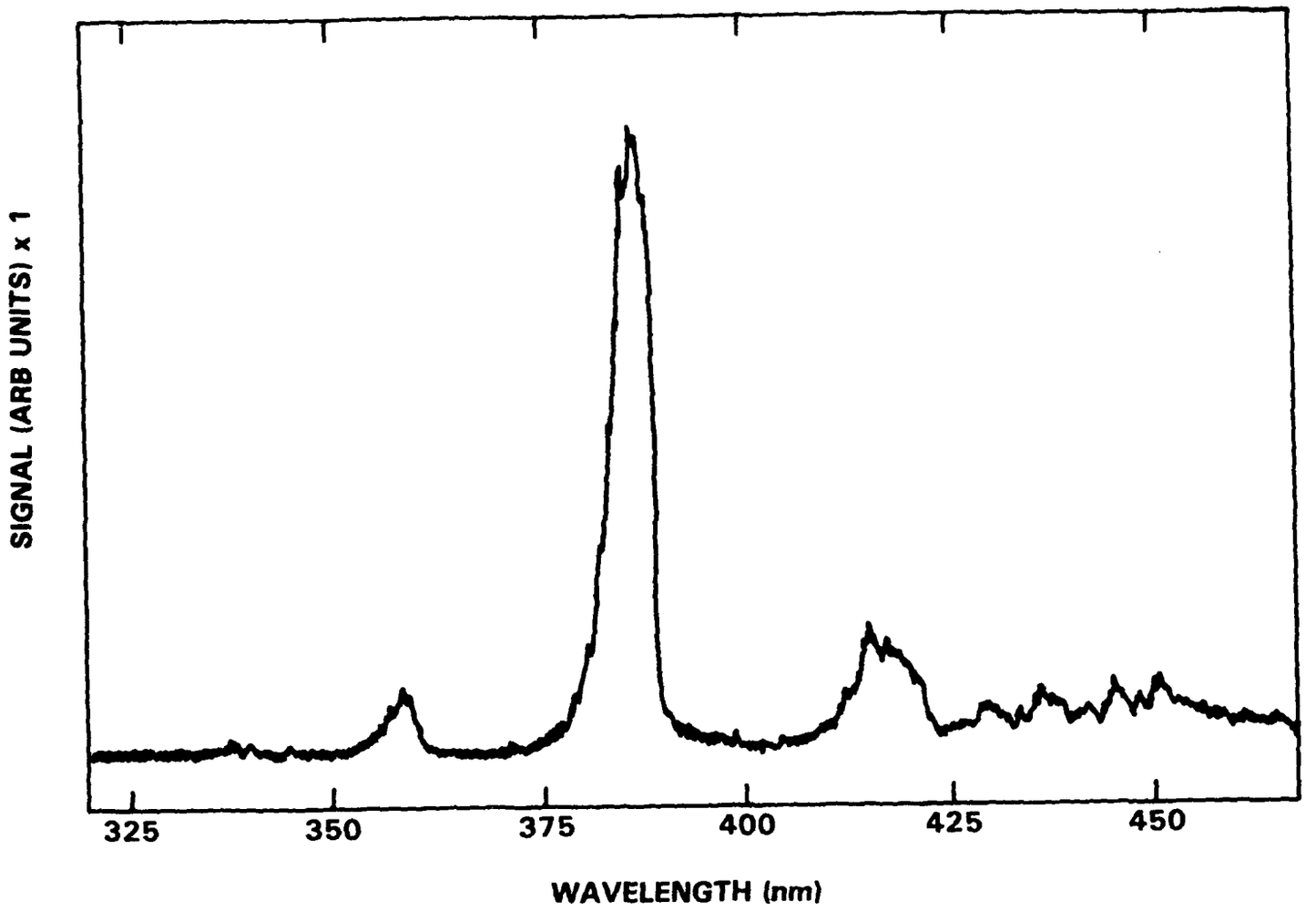

Fig. 24 Near-ultraviolet emission of cold trap purified FN_3 film detonation on plasma-clean SiO_2 substrate.

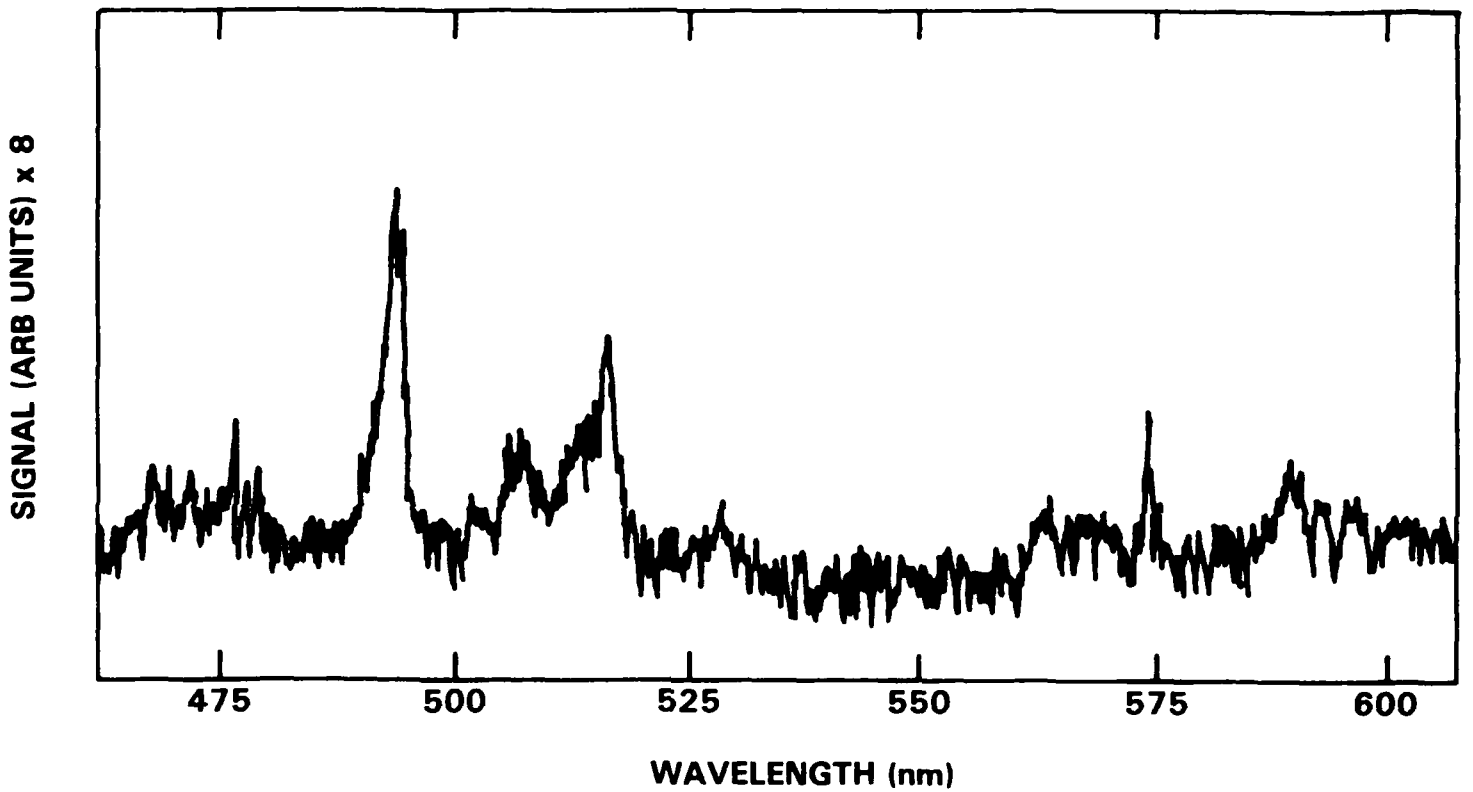

Fig. 25 Visible emission spectrum of cold trap purified FN_3 film detonation on plasma-cleaned SiO_2 substrate.

prior to radiation. When the FN_3 film is detonated, however, the molecular fragments are blown off into a vacuum and negligible thermalization occurs during the 10 μs aperture time of the measurement. Since the heat release and temperatures accompanying the detonation are large, it is reasonable to expect emission from the more highly excited vibrational levels of the NF(b) state.

Figure 26 shows the potential energy surfaces of NF, of which only the three lowest states ($X^1\Sigma$, $a^1\Delta$ and $b^1\Sigma$) are known experimentally.[23,24] The higher states were obtained by ab initio calculations performed by Michels[7] which also gave excellent agreement with the experimental data for the lower states. These results show that NF(b) is an excellent oscillator since there are no intersecting potential curves from the bottom of the well up to approximately 3 eV of vibrational excitation. Figure 27 shows a plot of the vibrational energy and the emission wavelength for the NF($b \rightarrow X$, $\Delta v = 0$) transitions vs the vibrational quantum number of the NF(b) state, which shows that if the mean vibrational energy of the NF(b) state were 1 eV, the NF($b \rightarrow X$) emission would be spread out from 528 to approximately 500 nm. A band, fitting this description in the visible emission spectra of the FN_3 film detonations (see Figs. 20, 23 and 25), can therefore be plausibly assigned to the NF($b \rightarrow X$) transition. Since there is little emission near 528 nm ($v' = 0 \rightarrow v'' = 0$ transition), the vibrational distribution of the NF(b) is strongly inverted. Inverted vibrational distributions of this type are well known to result from highly exothermic light atom abstractions as in the reaction of F-atoms with hydrogenated species.[25] How and why such distributions might appear in the detonation of FN_3, however, is at present unknown.

The above arguments, relative to potential vibrational excitation of the NF(b) state, can also be applied with equal validity to the NF(a) state, since it too is characterized by a deep potential well without intersecting potential energy curves (Fig. 26). Therefore, even though the NF($a \rightarrow X$) emission was not observed, it is reasonable to conclude that NF(a) is produced in a state of high vibrational excitation, since any reaction capable of generating NF(b) would also possess sufficient exothermicity and the proper spin quantization to yield NF(a) also.

Examination of the other visible and ultraviolet bands in the emission spectrum by comparison to the spectroscopic literature resulted in no clear assignments.[6] There was no $N_2(B \rightarrow A)$ emission as is normally observed in PbN_3 detonations[26] and no atomic

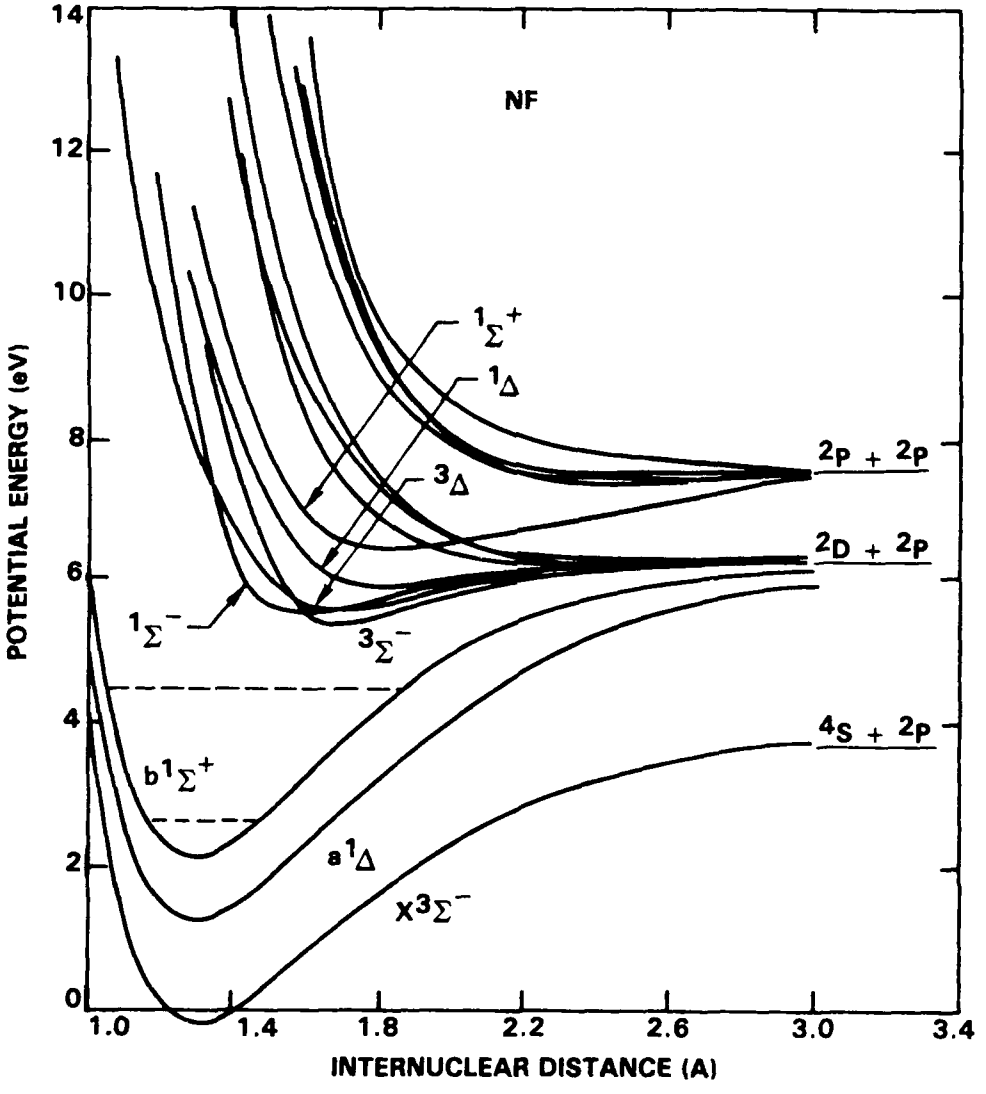

Fig. 26 Potential energy curves of NF. Only the lowest three states are known experimentally, the higher states were calculated by Michels.

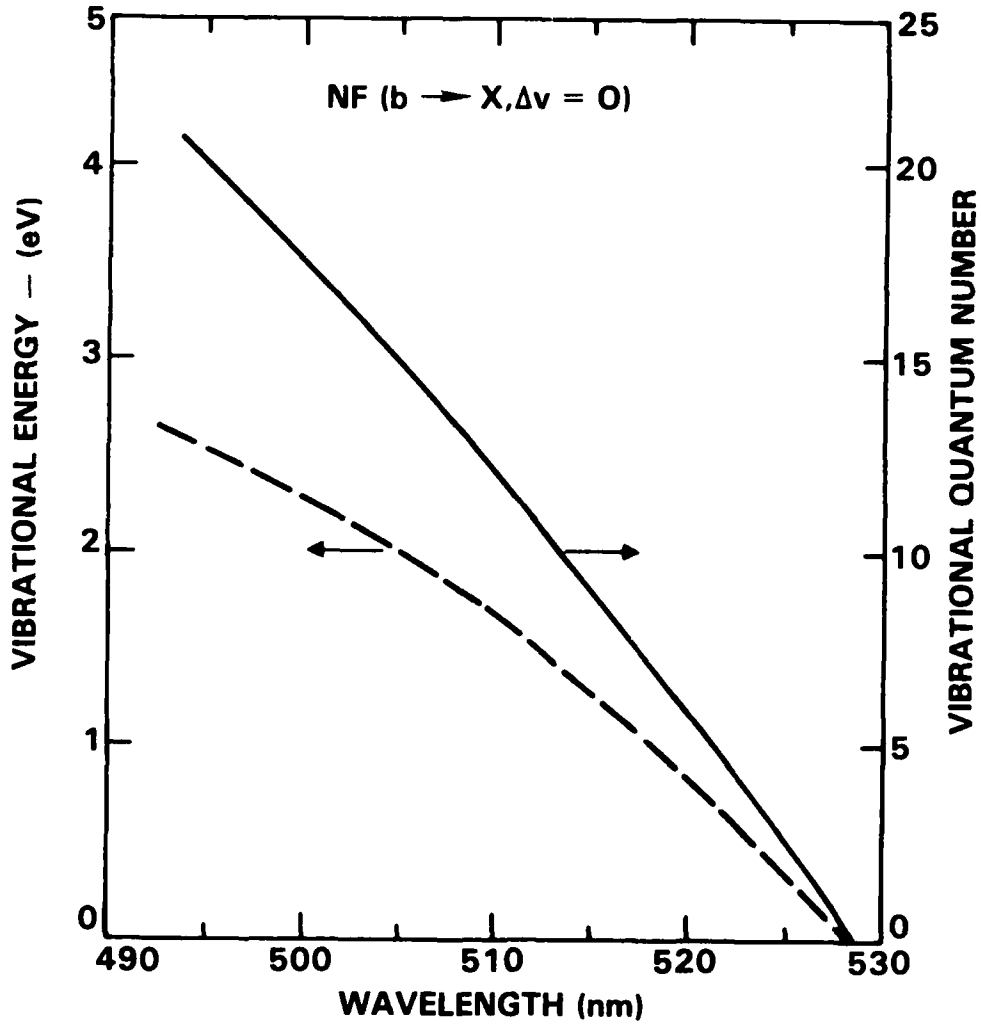

Fig. 27 Vibrational energy and quantum number of NF(b) vs wavelength of the $\Delta v = 0$ transition to NF(X).

emissions either. It was tempting to assign the ultraviolet bands below 400 nm to the $N_2(C \rightarrow B)$ band system since this corresponds to the N_2 laser transition and thus may be fluorescence, the bands are clearly diatomic with a regular vibrational spacing and the bands are violet degraded and at approximately the right wavelengths to agree with the literature.[6] Despite the similiarities, assignment of these bands to the $N_2(C \rightarrow B)$ transition is problematical, since if $N_2(C \rightarrow B)$ emission were significant, then $N_2(B \rightarrow A)$ emission would also be produced by radiative cascade, and none is observed.

A comparison spectrum, shown in Fig. 28, was generated by using the OMA and fiber optic cable to record the emission from a low pressure (1 torr) discharge in pure N_2, a known favorable source of $N_2(C \rightarrow B)$ emission.[6] A Hg lamp spectrum was also recorded to assure the accuracy of the wavelength calibration. Since the transitions examined all have a common upper state, $N_2(C, v' = 0)$, the relative intensities depend only on the Franck-Condon factors and are independent of the quenching environment. Also, since the same instrument was used to record both spectra, the wavelength dependence of the instrument response cancels out of the band to band relative comparisons. Assignment of the $N_2(C \rightarrow B, v' = 0 \rightarrow v'' = 0, 1, 2, 3)$ transitions was easily accomplished from the calculated bandhead positions. Comparison of the N_2 spectra in Fig. 28 to Figs. 19, 22 and 24 shows clearly that the ultraviolet emission from the FN_3 film detonations is not $N_2(C \rightarrow B)$. While the wavelengths are nearly correct, the intensity distributions are entirely different. The discharge source at 337 nm shows higher intensity, relative to the other bands than does the FN_3 detonation while the (0, 3) band is missing from the FN_3 detonation spectrum which should be clearly visible if the emission is $N_2(C \rightarrow B)$. Therefore, a different assignment is indicated for the ultraviolet emissions produced in the FN_3 film detonations.

Since the near-ultraviolet bands appear to be diatomic in origin and do not fit any of the known bands in N_2 or F_2, it is natural to assign these features to transitions in NF if impurities are eliminated. Examination of Fig. 26 shows that transitions from the more highly excited states of NF, around 6 eV excitation, to vibrationally excited energy levels of the NF(a, b) states can produce emissions at visible and near-ultraviolet wavelengths. Obase et al have reported observation of the $NF(c \rightarrow b)$ transitions from 440-570 nm upon reaction of NF_3 with metastable He in a discharge-flow system.[27] The

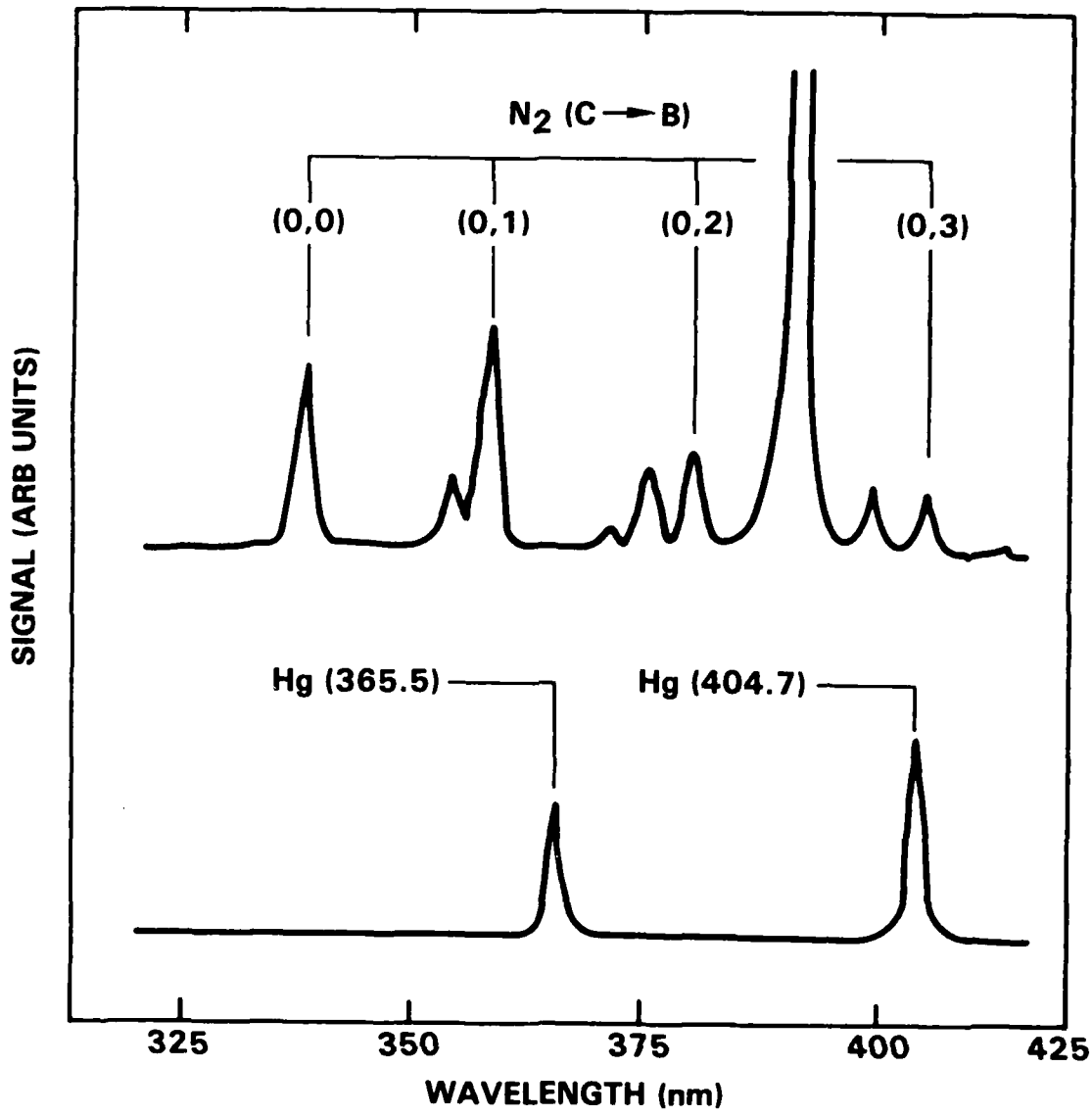

Fig. 28 Wavelength calibration (Hg lamp) and comparison spectrum (low pressure N_2 discharge).

spectrum obtained by these authors, however, does not agree with the data in Figs. 20, 23 and 25. The assignment by Obase, however, is disputed by other investigators[28] who have sought the NF(c → b) transitions by laser-induced fluoresence.

The NF(a) • NF(a) dimol emission is expected to occur near 437 nm (half the wavelength of the NF(a → X) transition) by analogy to the isoelectric O_4^* molecule.[29,30] Since this radiation only occurs while the NF(a) molecules are in a state of collision, the emission spectrum is typically without structure in contrast to the complex bands near 437 nm that are shown in Figs. 12, 22 and 24.

The bands at 387, 420 and 490 nm have only very recently been observed in a low-pressure flowtube experiment conducted in our laboratory as part of our IR&D program. Here, F-atoms are reacted with H_2 and FN_3 in the presence of various catalysts. The 387 and 420 nm bands are produced when hydrocarbons are added to the flow while the 490 nm band is best seen in the pure system. This result suggests that hydrocarbon impurities generated by outgassing of rough surfaces on the inside wall of the dewar may be a source of contamination. Outgassing of condensable impurities (hydrocarbons) was suspected because higher vacuum was obtained when the dewar was filled with liquid nitrogen, than when it was operated at room temperature. In this case, the emission bands at 356, 387 and 420 nm (Figs. 19, 22 and 24) could potentially be assigned to the CN(B - X) band system,[6] however, comparison spectra need to be generated to verify this conclusion.

The band at 490 nm appears to be the spectroscopic feature which is most characteristic of the FN_3 detonation, since it cannot be attributed to the presence of hydrocarbon impurities. Assignment of the 490 nm band to a transition in NF would require some modification of the potential energy curves that are shown in Fig. 26. Since the band in question is spectrally confined, vertical potential energy curves are indicated, while all of the states above NF(a,b) in Fig. 26 are displaced to larger internuclear separation. Consequently, assignment of this feature could be aided by a refined calculation of the NF potential energy curves.

Mechanism

Finally, we must address the potential reactions that are responsible for the observed emissions. If the visible/ultraviolet bands are assigned to transitions out of the higher states of NF, then energy pooling reactions must be invoked since these states lie too high to be directly accessed by FN_3 decomposition. Energy pooling is a special case of energy transfer from one excited state to another, resulting in the loss of energy from one molecule or atom with the corresponding production of a more highly excited state in the other. A good example of energy pooling occurs upon the reaction of two $N_2^*(A)$ molecules which produces one molecule in vibrationally excited levels of the $N_2(X)$ ground state and the other molecule in the higher N_2(B, C and C') states. Such reactions can occur with high probability and gas kinetic rates.[31] Therefore, one possible mechanism is

$$FN_3 \rightarrow NF^* + N_2 \qquad (1)$$

followed by

$$NF^* + NF^* \rightarrow NF(X) + NF^{**} \qquad (2)$$

where NF* are NF(a,b) molecules in a state of high vibrational excitation and the ultraviolet emissions are due to the radiative decay of the NF** species. Reaction (2) is not known experimentally because as Fig. 26 shows, collisions between the NF(a,b) molecules with $v \sim 0$, as generated by the prior sources, lack sufficient energy to populate the NF** states. The two dashed horizontal lines in Fig. 26 represent half the energy of NF** (lower line) and an upper limit to NF(b,v) produced in the detonations as inferred from the visible emission spectra (Figs. 20, 23 and 25) and the relationship between emission wavelength and vibrational energy (Fig. 27). Since there is a significant overlap region, we conclude that reaction (2) can occur following detonation of the FN_3 films and may be responsible for the ultraviolet emissions.

The production of the NF* molecules also requires a form of energy pooling to occur during the detonation process. Michel's has estimated[4] that the potential barrier

to dissociation of the FN_3 central bond is approximately 0.5 eV. Therefore, the detonation of FN_3 can be explained in terms of a branched chain reaction where NF(b) plays a significant role. In prior work,[2] we found that NF(b) is raidly quenched by FN_3. It is probable that NF(b) quenching by FN_3 yields NF(a) to conserve spin, thus the energy imparted to the FN_3 molecule could be as large as 1 eV, the NF(b - a) splitting.[6] Since this energy is greater than the FN_3 central bond energy, it is also likely that the FN_3 molecule will dissociate to NF(a,b) in the quenching reaction, thus giving rise to a chain. Such a chain reaction would not propagate, however, without a branching step to overcome NF(b) dissociation yields less than unity or other (quenching) losses of NF(b). Therefore, quenching of NF(a) by FN_3 with similar dissociation to NF(a,b) must also be invoked to explain the detonation reaction. The excitation[6] of NF(a), approximately 1.4 eV, is nearly three times the height of the barrier to FN_3 dissociation, thus a substantial amount of excess energy is available for partitioning into vibrational excitation of the product molecules. While this mechanism is not proven, it is physically plausible and consistent with our data. This argument however, does not rule out other mechanisms, based on compressive heating and thermal feedback, which have traditionally been used to explain detonation phenomena. Consequently, it is possible that the proposed "electronic" mechanism may coexist with other "thermal" mechanisms as either a major or minor channel for energy release.

From the standpoint of investigating stabilizer effects in Phase 3, it may not be critical to know the spectroscopic or kinetic details. Nonetheless, knowledge of these factors is still very important in terms of the selection of potential stabilizing materials and the generalization of the results obtained to other energetic systems. Collection of temporally resolved emission data is also expected to yield some clues on the identity and source of the various emitters. Therefore, as additional data is gathered, the spectroscopic assignments and kinetic mechanisms will be under continuous review. It is expected that continued collaboration with computational chemists will play a key role in the analysis of our results, since the existing base of experimental data is not easily related to the conditions of our experiment.

KINETIC INVESTIGATION (PHASE 2)

In this section, we develop the strategy for the next year's work based on the results obtained in the spectroscopic investigation (Phase 1). The primary goals of Phase 2 are to obtain kinetic information on the detonation of the FN_3 films to guide an interpretation of the mechanism and selection of stabilizing materials, and to develop a time-resolved diagnostic that can be used in Phase 3 to evaluate the approach to stability.

Issues and Methods

The assignment of the emission spectra and the interpretation of the underlying chemical mechanism hinge critically upon the elimination of impurities from the FN_3 films. Data collected in Phase 1 suggested that some of the ultraviolet emissions might be due to hydrocarbon contamination and hence assignable to the CN(B - X) band system. It is therefore necessary to perform additional experiments to check out this possibility before proceeding. Consequently, our first step will be to collect a sample CN(B - X) spectrum for comparison purposes. Under a parallel SDI contract,[32] we have studied the reaction of F-atoms with HN_3 and CH_4, and found it to be a favorable source of both CN(A - X) and CN(B - X) emission. The CN(A - X) band system has a large number of well-defined bands which make its assignment from the literature[6] straightforward. Moreover, the mechanism of this flame (F-atom stripping of HN_3 and CH_4 to yield free N_3 radicals and C-atoms, which then react with each other) is expected to produce both CN(A) and CN(B) on the basis of reaction exothermicity and molecular orbital correlations. Finally, the relative peak heights of the CN(B - X) band system from this source have been successfully correlated with the corresponding Franck-Condon factors and knowledge of the instrument response function. These findings lend considerable confidence to the spectroscopic assignment, however, the data were collected with a different spectrometer/detection system than was used in the coldfinger experiments. Therefore, to facilitate an equally valid comparison, we shall use the OMA detection system to record a sample CN(B - X) spectrum from the $F + HN_3 + CH_4$ flame. This procedure will facilitate direct comparison of the reference spectrum to the FN_3 detonation spectrum, without need to correct for instrument response. Mass spec-

trometer analysis of the FN_3/He gas stream will also be performed to determine if the generator output is contaminated by impurities, although this is not expected since cold trap variation had negligible effect on the detonation spectra. Finally, all rough surfaces on the interior of the dewar portion of the coldfinger apparatus will be turned down on a lathe to eliminate this potential source of contamination due to outgassing. Detonation spectra will then be collected and compared to Figs. 22 and 23 (under identical conditions) to evaluate the efficacy of this modification.

The principal kinetic issue is to determine whether the emissions are characteristic of the detonation itself or reactions between fragments in the gas cloud that is produced by the detonation. The time scale upon which the emissions occur can answer this question. The detonation velocity of FN_3 is unknown, but is expected to be very high, similar to PbN_3,[33] since the detonations are brissant and the heat release is large. Equating the heat release to the kinetic energy of the molecules yields a molecular velocity of approximately 10^6 cm/s. The time scale for burn through of a 10 μm-thick film is therefore approximately 1 ns. Since energy release requires increasing the internuclear separation, the detonation reactions do not occur in the film itself but rather at the surface of the film as the FN_3 molecules pass into the gas phase. The gaseous products that are produced also expand at a similar velocity, thus the density of the gas cloud is approximately $10^{21}/cm^3$ at 10 ns and falls to $10^{18}/cm^3$ at 10 μs. Reactions beetween molecules at $10^{18}/cm^3$ density will be significant on the 10 μs time scale, consequently, some discrimination can be achieved with μs resolution but ns resolution is ultimately required to get close to the initial detonation of the FN_3 film. Therefore, we will collect the kinetic data in three stages of increasing temporal resolution.

In the first stage, we will employ the existing instrumentation and gather temporal information for each emission band by varying the time delay and aperture time of the pulse generator which controls the gating of the OMA. By varying the delay time while holding the aperture time constant, information is gained regarding the fall time of the emissions. The rise time information is gained by holding the delay to its minimum while decreasing the aperture time. While these data are not highly accurate, they are easy to gather and will serve to establish the time base for more sophisticated diagnostics.

In the second stage, radiation from the detonation will be efficiently coupled to a photomultiplier tube (PMT) and inteference filter combination. The interference filter bandpass characteristics will be specified to match the bands of interest using the spectroscopic data gathered in Phase 1. The PMT will be coupled to a wide bandwidth storage oscilloscope triggered by the photodiode in the nitrogen laser beam. Cable delays will be used on the input line to assure that the storage oscilloscope is triggered in advance of the leading edge of the PMT signals. With a 50 MHz bandwidth on the storage oscilloscope, resolution down to 3 ns is theoretically possible. However, the achievable bandwidth will probably be limited by the intensity of the emissions obtained from the detonating films.

In the final stage, the detonating film will be probed by a low energy dye laser beam following prior detonation via the nitrogen laser, as shown in Fig. 29. In this technique, a fraction of the detonating nitrogen laser beam is split off to drive a small dye laser. The probe laser is constructed by placing a coumarin dye in a cuvette that is located at the line focus of a cylinder lens in the split off nitrogen laser beam. The dye will be selected to lase untuned at 420 nm so that the probing radiation will be absorbed by the FN_3 molecules. Since the FN_3 absorption band is broad and continuous, there is no need to precisely tune the dye laser. Consequently, a simple resonator consisting of two dielectric mirrors will be sufficient for generating the probe laser beam. Approximately 10% of the nitrogen laser beam or 100 μj will be outcoupled to the pump the dye laser. With typical conversion efficiencies, a dye laser output of approximately 5 μj is expected, sufficient to be easily detected by a silicon photodiode. The probing dye laser beam will be delayed relative to the detonating nitrogen laser beam by transmission through an optical trombone line. The delay is varied by moving the reflecting prism at the rate of about 0.06 ns/cm. The probing radiation is then directed through the detonating film to a filtered detector and the net charge produced by the detector is captured by a boxcar integrator. It is important to note that the resolution of this method is controlled only by the pulse width of the nitrogen laser (0.7 ns FWHM). The detector rise time and boxcar gate width can be selected for convenience. This diagnostic will give us a monitor of the film as it detonates on the ns time scale. Therefore, it should be very appropriate to the stabilization studies of Phase 3. Changes in the detonation velocity, detected by FN_3 absorption at selected times after detonation is initiated, will be a useful indicator of the influence of potential stabilizers.

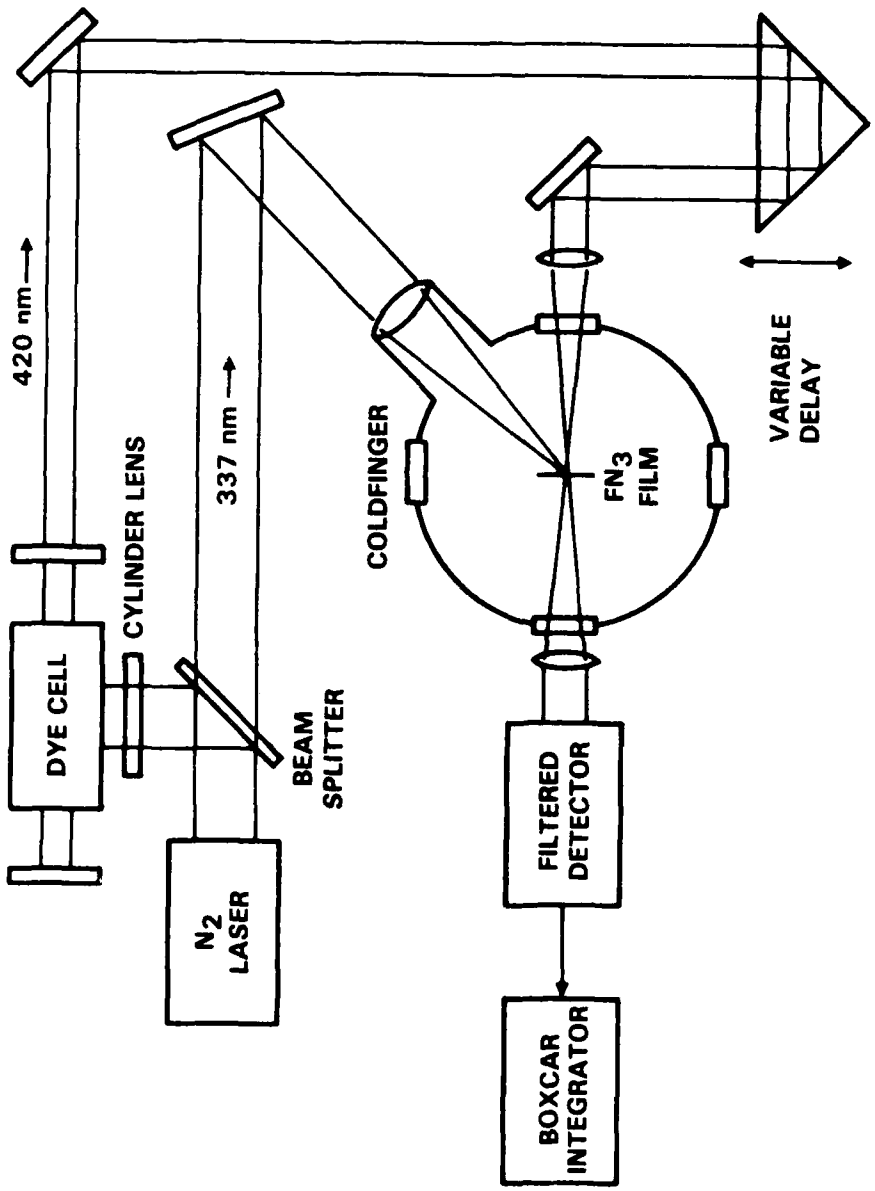

Fig. 29 Schematic of absorption diagnostic with 0.7 ns temporal resolution.

Program Plan

Figure 30 shows the schedule and tasks for Phase 2. In conducting the Phase 1 research, our level of effort was greater than planned. Therefore, we are at present slightly overspent on the contract and we have fallen behind schedule on other company-sponsored FN_3 projects. To correct these difficulties, we plan a two-month hiatus on the contract during August and September in which the level of effort will be held to a minimum. It is anticipated, however, that the coldfinger will be modified and the mass spectrum of the FN_3/He flow as well as the CN(B - X) reference spectrum will be gathered during this period. Following this, work will resume on Phase 2 in October at the nominal level of effort.

Since little effort is required to set up the gate variations and since only preliminary data is required from these experiments, only one month is planned for this activity. The experiments using the storage ocilloscope will also be easy to set up, but more extensive data will be required. Therefore, three months is planned for the collection of the time profiles. Finally, the absorption experiment will require some new construction and will have to be debugged. The data collection from these experiments will also be tedious since several shots will be required to generate each time history. Therefore, a full six months is planned for these most critical experiments with a milestone a three months for completion of an operational diagnostic capability.

Progress reports will continue to be issued on a quarterly basis, and a program plan for Phase 3 will be developed at the end of Phase 2. Finally, an oral viewgraph presentation will be delivered at the next High Energy Density Matter Conference.

Preliminary Results

The data presented in this section were collected during the hiatus period of Phase 2 and are reported here, in summary form, as an aid to the interpretation of the Phase 1 results. The reader is referred to the subsequent progress reports generated under this contract for further details regarding these measurements.

<u>CN(B -X) Emission</u> - The reference spectrum of the F + HN_3 + CH_4 flame precisely matched the FN_3 detonation spectrum (in the 350-425 nm range) as well as the spectrum

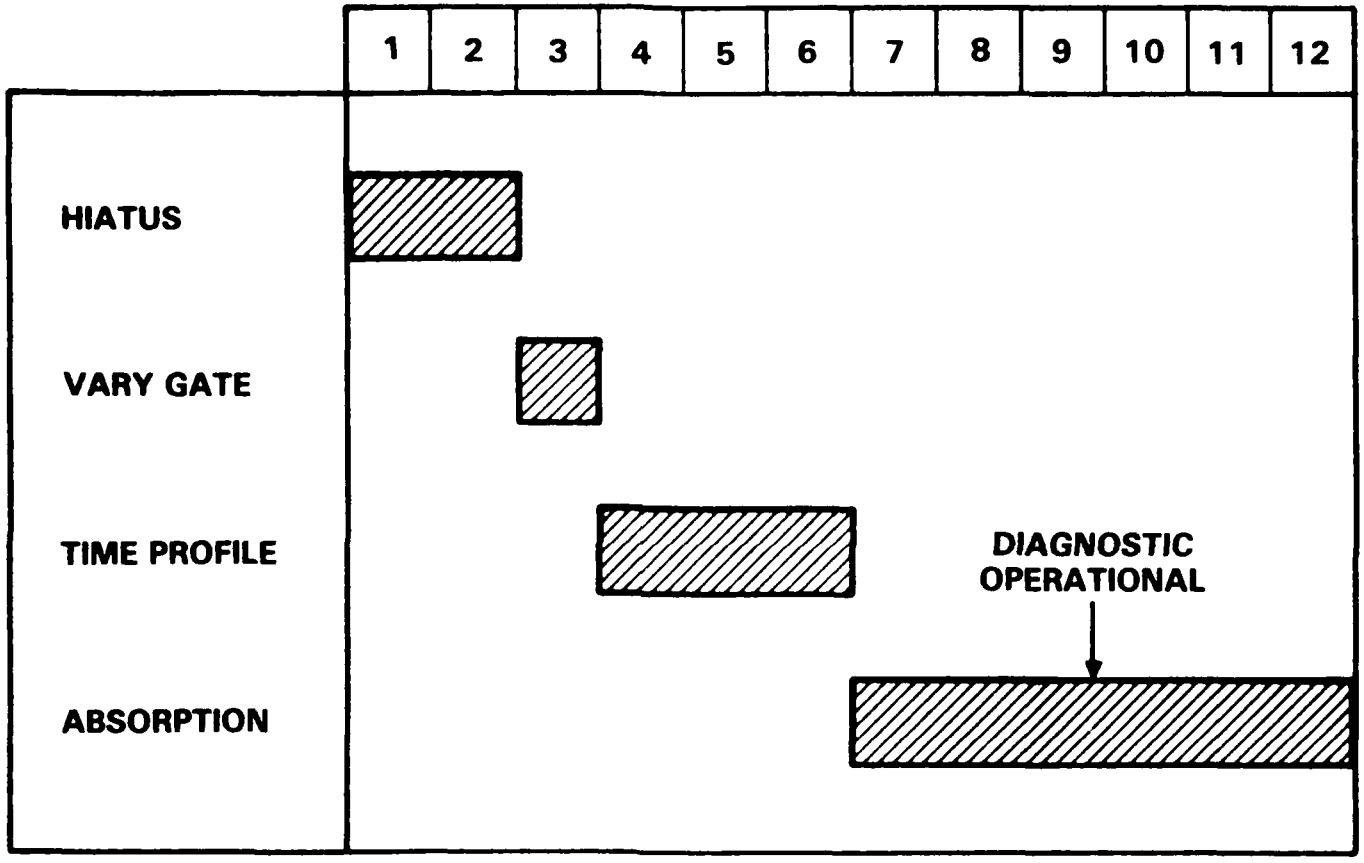

Fig. 30 Schedule for kinetic investigations (Phase 2).

of the $F + H_2 + FN_3$ + hydrocarbon flame in the flow tube reactor (in the 350-900 range). These results conclusively prove that the bands at 356, 387 and 420 nm in Figs. 19, 22 and 24 are due to the $\Delta v = -1$, 0 and 1 transitions of the CN(B - X) band system, respectively. It therefore follows immediately, that there is a source of carbon bearing impurities either in the FN_3/He gas stream or within the coldfinger apparatus itself. It is also interesting to note that while the $F + HN_3 + CH_3$ and $F + H_2 + FN_3$ + hydrocarbon flames each produced CN(A - X) as well as CN(B - X) emission, the FN_3 detonation spectrum contained only CN(B - X) emission. The absence of detectable CN(A - X) emission from the FN_3 detonations in the 500-800 m range (Figs. 20, 21, 23 and 25) shows that the mechanism of CN(B) production in the FN_3 detonation is different than in the flame systems. Chemical sources of excited CN, such as the $C + N_3$ reaction (in the flame systems), are likely to populate both the B and A states, since these are not differentiated by spin quantum number (analogous to the a and b states of NF). The selectivity exhibited in populating the CN(B) state in the FN_3 detonations can be explained by formation of ground state CN followed by resonant energy transfer from an excited precursor. Consequently, there is a suggestion, in these data, for the existence of a species with at least 3.2 eV of excitation in the FN_3 detonations, which pumps the CN(B) state by energy transfer. The vibrationally excited NF(a,b) states, previously referred to as NF*, are a likely candiate for this role.

Mass Spectra - Analysis was carried out using a quandrupole analyzer that was interfaced to the FN_3 generator via a leak valve. The genertor was operated in a variety of configurations to test for various impurities that might be present. No hydrocarbons were detected upon heating of stearic acid (without NaN_3 present), but a considerable amount of air was evolved during the initial warm-up. The outgassing of the stearic acid was complete, however, prior to the end of the warm-up period when experimentation was begun. When large amounts of NaN_3 were added to the stearic acid, a considerable amount of CO_2 was evolved along with the HN_3 during the latter portion of the run. The time profiles of the HN_3 and CO_2 signals were dissimilar, but were compatible with the absorption and flow data presented in Fig. 4. The amount of CO_2 evolved, however, was reduced considerably when the NaN_3 charge was limited to 0.1 mole per 2 moles of stearic acid, consistent with the absorption and flow data presented in Fig. 5. Since CO_2

has a higher vapor pressure[16] than FN_3, it is not removed from the flow by the cold trap, however, it is also unlikely that it condenses in significant quantities on the coldfinger. Titration of the F_2 with HN_3 produced the expected mass peak for FN_3 and very little N_2F_2, while passage of the FN_3 flow through a hot trap prior to the point of analysis eliminated the FN_3 signal entirely and produced an N_2F_2 signal of comparable magnitude. This result, which shows that very little N_2F_2 is produced as a by-product of the FN_3, was expected since thermal decomposition of FN_3 is known[1,3] to produce a high yield of N_2F_2. Although HN_3 and FN_3 each generated several peaks in the mass spectrum, which were expected, no peaks appeared at m/e ratios that were inconsistent with the known cracking patterns of these species.[3,34]

Coldfinger Modification - The rough surface in the dewar section of the coldfinger (indicated by * in Fig. 13) was turned down and the entire coldfinger apparatus was cleaned and reassembled. These changes significantly attentuated the CN(B - X) emissions, confirming the hypothesis that hydrocarbon outgassing was the indicated source of contamination in the FN_3 films.

Gate Variations - Preliminary data was collected in the 320-470 nm range (after the coldfinger modification) with gate delays of 0.1 and 10 μs and gate widths of 10 and 50 μs. These studies showed two overlapping spectral features in the 400-460 nm range with different time profiles. One feature, centered at 430 nm, was without structure and attenuated rapidly during the first 10 μs after detonation, while the other feature showed a regular series of red degraded bands peaking at 445 nm, which grew significantly in intensity between 10 and 50 μs after the detonation. From these observations, we may conclude that the structured feature arises due to secondary reactions between the gaseous products of the detonation. Greater temporal resolution will be required, however, to determine whether the unstructured feature is due to primary or secondary reaction products. Nonetheless, it is interesting to note that this feature could be explained by NF(a) • NF(a) dimol emission since it is unstructured and appears at half the wavelength of the NF(a - X) transitions. Since dimol emission intensity is proportional to the square of the NF(a) concentration and the volume of the gas cloud while the product of the NF(a) concentration and the volume of the gas cloud tend to remain constant, the

intensity of the dimol emission is expected to fall off rapidly as the gas cloud expands, consistent with our observations. Furthermore, for high initial NF(a) concentrations and short aperture times, the intensity of the dimol emission may be large compared to the intensity of the NF(a - X) emission. Consequently, there is no contradiction in observing the dimol band when the NF(a - X) emission is too weak to detect. Further studies of this potential dimol emission band with greater temporal resolution are therefore warranted, since it may provide a useful diagnostic to monitor the detonation at very short times.

REFERENCES

1. J.F. Haller, Ph.D. Dissertation, Cornell Univerzsity, 1942.

2. D. Patel, A.T. Pritt and D.J. Benard, J. Phys. Chem. 90 (1986) 1931.

3. K. Gholivand, G. Schatte and H. Willner, J. Inorg. Chem., to be published.

4. H.H. Michels, United Technology Research Center, private communication.

5. D.J. Benard, Science Center proposal SC4339T (1987), to be published.

6. B. Rosen, Spectroscopic Data Relative to Diatomic Molecules, Pergammon Press (New York).

7. H.H. Michels, United Technology Research Center Report No. 77-05-236-8.

8. N.I. Sax, Dangerous Properties of Industrial Materials, Sixth Edition, Van Nostrand (New York).

9. J.T. Baker Chemical Co., Material Safety Data Sheet No. S2906-01.

10. Matheson Gas Products, Technical Brief No. TB-115.

11. B. Krakow, R.C. Lord and G.O. Neely, J. Mol. Spectroscopy 27 (1968) 148.

12. J.R. McDonald, J.W. Rabalais and S.P. McGlynn, J. Chem. Phys. 52 (1970) 1332.

13. D.A. Dows and G.C. Pimentel, J. Chem. Phys. 23 (1955) 1258.

14. L.G. Piper, R.H. Krech and R.L. Taylor, J. Chem. Phys. 71 (1979) 2099.

15. Pye-Unicam Model 6-550 UV/VIS Spectrophotometer.

16. R.C. Weast, Handbook of Physics and Chemistry, CRC Press (Cleveland).

17. C.B. Childs, Appl. Optics 1 (1962) 711.

18. R.J. Malins and D.W. Setser, J. Phys. Chem. 85 (1981) 1342.

19. R.D. Combe, Final Report of AFWL Contract No. F29601-79-C-0016, September 1981.

20. P.H. Tennyson, A. Fontijn and M.A.A. Clyne, Chem. Phys. 62 (1981) 171.

21. K.A. Mohammed, B.N. Khanna and K.M. Lal, Ind. J. Pure Appl. Phys. 25 (1974) 221.

22. A.T. Pritt and D.J. Benard, J. Chem. Phys. 85 (1986) 7159.

23. W.E. Jones, Can. J. Phys. 45 (1967) 21.

24. A.E. Douglas and W.E. Jones, Can. J. Phys. 44 (1966) 2251.

25. S. Wategaonkar and D.W. Setser, J. Chem. Phys. 86 (1987) 4477.

26. S. Rosenwaks, Beer-Sheva University, private communication.

27. H. Obase, M. Tsuji and Y. Nishimura, Chem. Phys. Lett. 126 (1986) 134.

28. R.A. Young, Rockedyne, private communication.

29. J.S. Arnold, E.A. Ogryzlo and H. Witzke, J. Chem. Phys. 40 (1964) 1769.

30. L.W. Bader and E.A. Ogryzlo, Disc. Faraday Soc. 37 (1964) 46.

31. G.N. Hays and H.J. Oskam, J. Chem. Phys. 59 (1973) 1507.

32. M.A. Chowdhury and D.J. Benard, Quarterly Progress Reports No. 7 and No. 8 of SDIO/OIST (LANL) Contract No. 9-X25-X1451-8 (1987).

33. M.M. Chaudri, W.L. Garrett, O. Sanders and N. Slagg, Propellants and Explosives 2 (1977) 91.

34. A. Cornu and R. Massot, Compilation of Mass Spectral Data, Haydon & Sons Ltd. (France).

END

DATE

FILMED

8-88

DTIC